



جامعة المجمعة
Majmaah University

JEAS



JOURNAL OF ENGINEERING — AND — APPLIED SCIENCES

A Refereed Academic Journal Published by the
Publishing and Translation Center at Majmaah University

Vol. 3 Issue (2)

(November 2016)

ISSN: 1658 - 6638



Publishing & Translation Center
Publishing and Translation Center - Majmaah University

**IN THE NAME OF ALLAH,
THE MOST GRACIOUS,
THE MOST MERCIFUL**

**Kingdom of Saudi Arabia
Ministry of Education
Majmaah University**



JEAS

**JOURNAL OF
ENGINEERING
— AND —
APPLIED SCIENCES**

**A Refereed Academic Journal Published by the
Publishing and Translation Center at Majmaah University**

Vol. 3, Issue (2)

(November 2016)

ISSN: 1658 - 6638



Publishing & Translation Center - MU

About the Journal

Journal of Engineering and Applied Sciences (JEAS)

Vision

Pioneer journal in the publication of advanced research in engineering and applied sciences.

Mission

A peer-review process which is transparent and rigorous

Objectives

- a) Support research that addresses current problems facing humanity.
- b) Provide an avenue for exchange of research interests and facilitate the communication among researchers.

Scope

JEAS accepts articles in the field of engineering and applied sciences. Engineering areas covered by JEAS include:

Engineering areas

Architectural Engineering
Chemical Engineering
Civil Engineering
Computer Engineering
Electrical Engineering
Environmental Engineering
Industrial Engineering
Mechanical Engineering

Applied Sciences areas

Applied Mathematics
Applied Physics
Biological Science
Biomathematics
Biotechnology
Computer Sciences
Earth Science
Environmental Science

Correspondence and Subscription

Majmaah University, Post Box 66, AlMajmaah 11952, KSA

email: jeas@mu.edu.sa

© Copyrights 2016 (1438 H) Majmaah University

All rights reserved. No part of this Journal may be reproduced or any electronic or mechanical means including photocopying or recording or uploading to any retrieval system without prior written permission from the Editor-in-Chief.

All ideas herein this Journal are of authors and do not necessarily express about the Journal view

Journal of Engineering and Applied Sciences

Editorial Board

Dr. Sameh Saadeldin Ahmed, Editor-in-Chief

Associate Professor, Civil and Environmental Engineering Department, College of Engineering, Majmaah University

Dr. Adel Zaki, Member

Professor, Mathematics Department, College of Science, Zulfi Campus, Majmaah University

Dr. Syed Mohammad Abbas, Member

Professor, Civil and Environmental Engineering Department, College of Engineering, Majmaah University

Dr. Waqar Ahmed Khan, Member

Professor, Mechanical and Industrial Engineering Department, College of Engineering, Majmaah University

Dr. Abdul Majid Abdul Majeed, Member

Professor, Physics Department, College of Science, Zulfi Campus, Majmaah University

Dr. Bhanu M. Bhaskara, Member

Professor, Computer Engineering, College of Computer and Information Sciences, Majmaah University

Dr. Mohammad Kashif Uddin, Secretary

Assistant Professor, Basic Engineering Sciences Department, College of Engineering, Majmaah University

Editorial

Scientific publishing has brought many challenges to authors. With increasing number of scientific journals, varying scopes and reviewing requirements, and cost of publishing to authors, finding the right journal to publish an article is a decision many authors must bitterly confront and resolve. The publication of scientific findings is an integral part of the life of researchers; and the process of publishing has evolved to become an efficient system of decimating knowledge and collaboration among scientists. Science journals have institutionalized procedures to manage large volume of article submissions per year; in many cases, journals began to define narrower scopes for a dual purpose: managing submissions and delivering outstanding research.

Based on recent studies, the scientific publishing world consists of more than 25 thousands active journals in various disciplines and fields. Science Direct hosts 3,348 journals (as of February 2014). The Directory of Open Access Journals lists in its search engine more than 9,800 open access online journals.

According to recent estimates, the number of scientific journals grows by 3% per year worldwide. With this large number of journals, journals may find it harder to stay afloat.

In its inauguration, the board of editors is honored to introduce to the scientific community the Journal of Engineering and Applied Sciences - JEAS, another scientific journal from Majmaah University. The board has pledged a commitment to JEAS authors and readers to bring the most dynamic and vibrant journal management with better satisfaction.

Dr. Sameh S. Ahmed

Contents

Editorial..... vii

ORIGINAL ARTICLES

Space Air- Conditioning by Aqua Ammonia Absorption System using Exhaust Waste Heat of Diesel Generator Set

Vakkar Ali and Ziaur Rehman1

Synthesis, Characterization and Efficiency of Alum Produced from Waste Aluminium Cans for Wastewater Treatment

A.L. Adejumo et al.8

Concomitant Administration of Quercetin and α -tocopherol Protects Rats from Cadmium Chloride Induced Neural Apoptosis and Cognitive Dysfunction

Ali A. Shati.....14

Structural Investigation of Semi Crystalline LDPE Nano-polymer

M. S. Gaafar, H. Afifi and Kh. Al Zenidy24

The Photogravitational Circular Restricted Four-body Problem with Variable Masses

Abdullah A. Ansari.....30

Space Air- Conditioning by Aqua Ammonia Absorption System using Exhaust Waste Heat of Diesel Generator Set

Vakkar Ali

Department of Mechanical and Industrial Engineering, Majmaah University, Majmaah, Kingdom of Saudi Arabia,

w.ahmad@mu.edu.sa

Ziaur Rehman

Department of Civil and Environmental Engineering, Majmaah University, Majmaah, Kingdom of Saudi Arabia,

z.rehman@mu.edu.sa

Abstract

The present work is an experimental analysis for space air conditioning system. The absorption system is using the exhaust waste heat energy of a diesel generator engine of 11.20 kW. The present study is carried out to use waste heat energy in an absorption air-conditioning system. A wooden test room of 3.375 m³ capacity is built to simulate the air-conditioned space. The obtained results show that performance of the system in terms of COP decreases with increase in condenser and absorber temperatures and is directly proportional to the generator and evaporator temperatures of the space air-conditioning system. The condenser, evaporator and absorber temperatures of the system are recorded and it is found that the effect of these temperatures on COP of the air-conditioning system ranges 0.64 to 0.94. It was found that the designed air-conditioning system is capable of generating the estimated cooling load without consuming extra energy. The main advantage of the system is low operational cost of air-conditioning system and environmental hazards.

Keywords: Aqua Ammonia; Absorption system; Exhaust gas heat; Space Air-conditioner; Waste heat.

1. Introduction

Energy sources in Saudi Arabia describe petroleum production, consumption and export, but also natural gas and electricity production. Saudi Arabia is the world's largest crude petroleum producer and exporter. The 90% of the total country export and 75% revenues [1] depend on the petroleum products. The economy is still very dependent on oil in spite of diversification efforts, in especially petrochemical industry. In 2011, the export was 10.82 million barrels per day (1.7142×10^6 m³/d) of petroleum [1]. While most of this is exported, along with domestic use is rapidly increasing, primarily for electricity production and automobile transportation sector but the large portion of the oil is being used for domestic electricity demand in the country. As of January 2007, Saudi Aramco's proven reserves were estimated at 259.9 billion barrels (41.32×10^9 m³), comprising about 24% of the world total [2], 85% of the Saudi oil fields found have not produced oil yet, it would last for 90 years at the above said rate of production. Some energy experts are convinced that the current reserves are substantially lower than those officially claimed by Saudis and that the depletion rate is substantially faster [3]. The Kingdom's consumption of its own oil production has steadily increased and it now consumes about one quarter of its oil production (approximately three

million barrels per day) [3]. According to Jim Karne, 'Saudi Arabia now consumes more oil than Germany', an industrialized country with triple the population and an economy nearly five times as large' [3, 4]. The only way to reduce energy consumption would be to reduce input in energy producing devices or systems. Saudi Arabia is the fastest growing electricity consumer in the Middle East, particularly of transportation fuels. In 2005, Saudi Arabia was the world's 15th consumer of primary energy, of which over 60% was petroleum based. The remainder was made of natural gas [5]. The Saudi Government has approved the construction of a \$300 million facility to turn waste into energy. The facility will process 180 Tons of waste per day, producing 6 MW of electricity and 250,000 US gallons of distilled water [6], therefore it is clear that the country is really thinking in the direction of waste energy saving schemes. The carbon dioxide emissions also increasing day by day in the country due to highly consumption of petroleum products in 2009 the country was the 15th top carbon dioxide emitter per capita that was 18.56 tons per capita [7].

Therefore, the country dependence on petroleum products for long term should be decreased as much as possible to move towards the use of renewable energy or the optimal use of waste energy sources. Moreover,

extensive use of fossil results in environmental hazards like global warming, greenhouse effect, depletion of ozone layer, climate change and acid rain. The future scenario of Saudi Arabia is full of use renewable, waste and others alternative sources of energy. In stationary diesel engine like diesel electric generator about 33% waste heat energy goes with exhaust gas of the engine, this energy could be useful to run many thermal system, like heat exchanger, vapor absorption generator and boiler to heat the working fluid and use it for useful work. The shaft work in mechanical compressor requires energy so that increases the on the engine, therefore an increase in fuel consumption, exhaust emissions, and engine operating parameters. Using waste heat of the engine we can save fuel consumption as well as the impact of emissions on the global environment.

Table 1: Energy in Saudi Arabia

Year	Capita Million	Primary Energy TWh	Production TWh	Export TWh	Electricity TWh	CO ₂ Emission Mt
2004	24.0	1,633	6,469	4,811	148	324
2007	24.2	1,748	6,412	4,606	175	358
2008	24.7	1,879	6,734	4,796	187	389
2009	25.4	1,836	6,145	4,324	199	410
2010	27.4	1,969	6,258	4,551	219	446
2012	28.08	2,176	6,998	4,700	227	457
Change 2004-10	14.6%	20.6%	-3.3%	-5.4%	48%	37%

Nomenclature:

- m = mass flowrate of exhaust gas, kg/s
- C_p = specific heat, kJ/kg °C
- T_o = outlet temperature, °C
- T_i = inlet temperature, °C
- T_g = generator temperature, °C
- T_c = condenser temperature, °C
- r.p.m. = revolution per minute
- COP = coefficient of performance
- Q_{gen} = heat generated, kW
- Q_{evap} = amount of heat absorbed in the evaporator, kW

2. Literature Review

Diesel engines are mostly used for power

generation due to their low cost and high thermal efficiency. Diesel engines have become popular for their use in all type of power generation stations [8]. Many scientists have been studied power generation plant with other energy saving plants using C.I. engines.

Many researchers conducted studies on absorption air-conditioning using waste heat energy Robert and Frosch [8]. Bingahadi *et al* [9], Franket *et al* [10], Alhuseinand Inayatullah [11] fabricated and designed a simple aqua ammonia absorption system automobile air- conditioning using the waste heat of exhaust from a S.I engine. Gui *et al* [12] and Masadeh [13] investigated aqua ammonia air-conditioning system for automobile utilizing the exhaust energy of a S.I engine. Al-Aqeeli and Gandhsadan [14] analyzed the feasibility and design of an air conditioning system for automobile using the absorption approach with LiBr-H₂O as working fluid. Shah Alam [15] studied a model of air-conditioning system using the exhaust waste heat of four cylinder four stroke passenger car and used three working fluid (NH₃, H₂, and H₂O) in vapor absorption system. Silva *et al* [16]. Crepinsek *et al* [17] studied the performance of different working fluid used in absorption air-conditioning cycle for mobile system [18]. It is clear from the investigations of many researchers result to absorption refrigeration systems only few researchers studied the possibility of using waste heat of internal combustion engine for useful work as absorption refrigeration systems because, in the present era a large amount of waste heat energy is released to the environment without using for beneficial work [19-20].

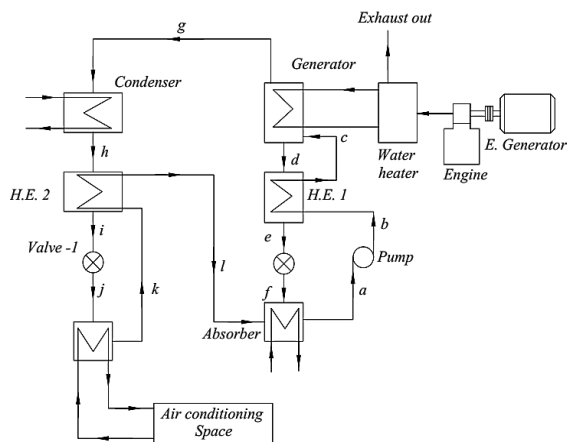


Fig. 1: schematic diagram of absorption system coupled with electric diesel generator

It is well none from the available literature and investigations of the researchers that utilization of

waste heat from the internal combustion engine for absorption air conditioning system. A large amount of research papers has been published on the use of waste heat from diesel engine and few only attempts have been made to attach the air-conditioning system to the small diesel power generation units like 20-30kW capacity. Hence, the main purpose of this present work is to see the feasibility to utilize the waste heat energy of a 20 kW diesel engine electric generator for the vapor absorption air-conditioning system and to replace the conventional vapor compression system for air-conditioning purpose. The feasibility of such type air-conditioning systems with large scale diesel power plants in Saudi Arabia will be advantageous in coming future to reduce the fuel consumption, adverse impact of emission on environment and make the power systems more economic. The proposed electric load for the year 2018 is 51,200 MW [21] and approximately 20--30 % of this energy is going with exhaust gas which is a huge amount of energy that can be utilized for useful work to reduce the consumption of fossil fuels up to some extent and harmful emissions to the environment. The main refrigeration cycle load can be reduced by using the waste heat energy of diesel engine and get two advantage such as cooling effect as well as reduction in emissions.

3. System Description

The complete schematic diagram of absorption air conditioning system with 11.20 kW diesel engine electric generator is shown in Fig. 1 (specification see in Table 2) which installed in the Mechanical Engineering laboratory of Al-Falah College of Engineering and Technology, Dhauj Faridabad, Haryana, India and used for the said experiment. The absorption air-conditioning system uses a binary mixture of ammonia and water and both referred as refrigerant and absorber having high stability for a wide range of operating conditions temperature and pressure. The system performance is highly dependable on the refrigerant latent heat of vaporization of ammonia. In this system, two heat exchanger with rectifying column are used to improve performance. The generator is used to generate the ammonia vapor using the waste heat of diesel engine and rectified with the help of rectifying column installed near it. The strong solution of ammonia and water from the absorber at state (a) is pumped to the condensing pressure level and preheat it in the heat exchanger to reduced heating at state (c).



Fig. 2: Photo Image Diesel Engine with Electric Generator

The hot water heated by the exhaust gas of the engine is fed in to the generator to heat the strong solution of ammonia and water and the weak solution goes to the rectifying column at state (d) and the ammonia at state (g). The weak solution of ammonia and water is fed to heat exchanger and then flows through the expansion valve and finally goes to the absorber at State (f). The ammonia vapor is fed to the air cooled condenser at state (g) for cooling. The condensate enters the heat exchanger for cooling further up to a state (i) and then goes to the expansion valve. In the expansion valve, the pressure is reduced to evaporator pressure level and then fed to evaporator at state (j) here the liquid refrigerant absorbs the heat and changes the phase due to absorbing latent heat of vaporization and produces cooling effect for required air conditioning system. After passing through the evaporator the refrigerant is further heated in heat exchanger-2 at state (l) and then is fed to the absorber for the next cycle.

Table 2: Diesel engine specifications of electric generator

S.No.	Name of parameter	Quantity
1.	Name of Company	Shakti Man, Single phase, 220 V, 50Hz
2.	Number of cylinder	1
3.	Type	Vertical cylinder
4.	Cooling	Water cooled
5.	Capacity	11.20 kW
6.	R.P.M.	1050
7.	Compression ratio	17:1
8.	Bore size	1.7 mm

3.1. Thermal analysis for experimental investigation

The experiment was conducted in the laboratory of department of Mechanical Engineering at Al-Falah College of Engineering and Technology, Dhauj Faridabad, Haryana, India. The air-conditioning space which has 800 cubic feet volume was found satisfactory or comfort cooled and the load was estimated 1.25 ton [14] of refrigeration for outside temperature 45°C and 25°C as the inside temperature range. The cooling load of the space is almost constant and design for 3 persons sitting and doing work on computer was found 2.43 kW. The room was perfectly insulated with thermocol sheet and not exposed to the sun from any side. The cooling load capacity is measured in kW which is the heat amount removed from the air-conditioning space. The exhaust gas heat is being utilized as an energy source input to generator of the absorption system. The amount of heat energy using for heating the water in cross flow heat exchanger can be estimated by [19, 20] using the below relation.

$$Q_{\text{gen}} = mC_p (T_o - T_i) \quad (1)$$

The analysis of absorption cycle Fig. 1, the heat flow from each component shows and thermal calculations for heat transfer results were done for the comparison to the reported work found in literatures. In absorption system the cooling effect is produced in the evaporator which termed as Q_{evap} (amount of heat absorbed by the refrigerant). The coefficient of performance of said absorption cycle [20] is given by below relation.

Coefficient of performance (C.O.P.) = Heat absorbed in evaporator/ Heat given to the generator

$$\text{C.O.P.} = \frac{Q_{\text{evap}}}{Q_{\text{gen}}} \quad (2)$$

where, Q_{evap} is the amount of heat absorbed in the evaporator refrigerant and Q_{gen} is the amount of heat given to the generator for heating the ammonia water solution.

The denominator is more important for the thermodynamic analysis and coefficient of performance because this heat is recovered of waste heat of exhaust gas of the diesel engine.



Fig. 3: Photo Image of waste heat absorption system

4. System specifications and design

In vapor compression system the compressor is used to increase the temperature and pressure of refrigerant vapor up to the stage of condenser while in vapor absorption system the same activity is done by the generator where the waste from the exhaust is utilized. The generator absorbs the heat of hot water heated by the waste gas and heats the strong solution of $\text{NH}_3 + \text{H}_2\text{O}$, and evaporates the ammonia from the mixture and then fed to condenser. The main factor in system design especially for generator is which is relatively large than vapor compression system. The designed dimension is shown in the Table 1. The actual details of design and consideration will not be shown in presented paper because limitations are not allowed to explain in wide range. The relations, Correlation and thermodynamic analysis for the whole system are taken from the references [15, 17, 18, 19, 20]. The generator takes the heat the heat from hot water coming from water heater at 95°C for this purpose a shell and tube heat exchanger is used with 32 tubes and having 1.25 cm diameter made by copper. The exhaust gas is used to heat the water in the heat exchanger. Now the hot water of the heat exchanger is being fed to generator to heat ammonia water solution. The exhaust gas exhausted to the atmosphere directly after using its heat in the water heat exchanger. The condenser is cooled by the water available in the laboratory at room temperature. The specification of various components like vapor absorption assembly, capacity of generator, generator pressure, tube length, overall heat transfer coefficient, total heat transfer area and generator temperature are given in the Table 3.

Table 3: System specifications

S.NO.	Name of item	Dimension
1.	Vapor absorption assembly with generator	Length-75cm,Width-45cm and height- 25 cm
2.	Generator heating capacity	3.516 kW
3.	Generator temperature	95 °C
4.	Generator pressure	2×10^6 Pa
5.	Over all heat transfer coefficient U	6.892 W/m ² °C
7.	The total heat transfer Area A	0.3489 m ²
8.	Tube length	5.98 m

5. Results and Discussion

When the system is operated for air-conditioning purpose the generator-set is started. The analysis is carried out when the performance of the diesel engine is stabilized. Otherwise the results may be affected and deviated up to some extent. In this attempt the effect of engine load, exhaust gas temperature, exhaust flow rate and engine speed on the performance of space air conditioner are analyzed. The performance of the space air-conditioner will be affected by the temperature of evaporator (Cooling coil), generator, absorber, and condenser. The temperature of flue gasses is directly proportional to the speed of the generator engine and also flow rate increases with increase in speed. The energy with the exhaust gasses affects the performance of air conditioning system. It is depicted from Fig. 2, the energy and temperature of the exhaust gasses is directly proportional to the engine generator engine speed also clear that cooling effect of the system increases with increase if generator set speed. The variation in increment of the gas temperature and energy will not be continued more after speed of 1000 r.p.m. This is because of the maximum rate of evaporation of ammonia in the generator that imposes the limit on heat supply to generator and further change in positive direction of heat input to the system would not be beneficial to increase the performance for the space air-conditioning system. Another disadvantage at higher speed of generator set engine is more wear and tear in the moving parts which is again responsible for cost factors. It is generally found that electric generators are used for peak loads and high speed of engine most of the time. Therefore, the performance

of system will not be affected more at moderate speeds of generator set engine. Hence it is advisable to get optimized value of performance (Cooling effect) of the system to run the engine at moderate engine load and speed.

It is depicted from Fig. 4 that the exhaust gas temperature increases with increase the generator engine load and speed meaning that more heat will be given to the system. It is seen from the results for load ranging from 25% to 75% on the generator set engine, the exhaust gas maximum temperatures are 235 °C and 275 °C respectively. This range of temperature is quietly more than the temperature available at the speed ranging from 600 to 1100 r.p.m.

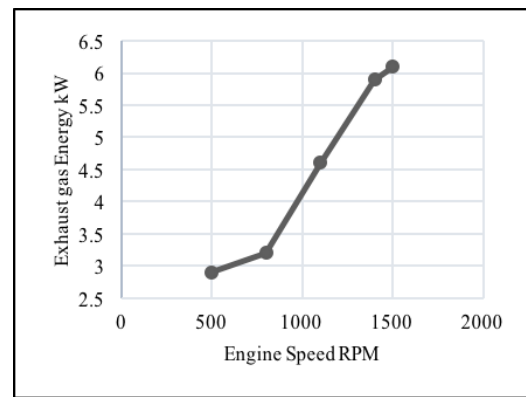


Fig. 4: Variation of diesel engine speed with the exhaust heat generation

It has been shown from Fig. 5 that the heat of generator increases with increasing the exhaust gas temperature. As equation 2 shows, the higher the value of Q_g lower the value of C.O.P of air conditioning system.

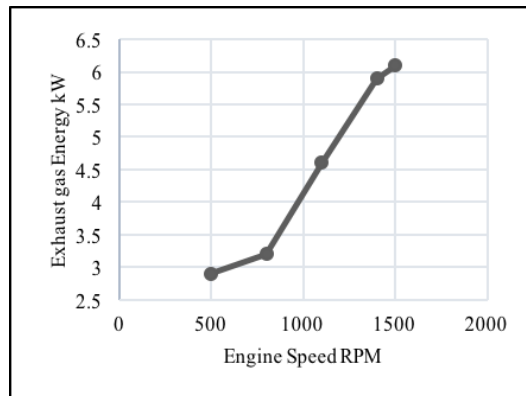


Fig. 5: Variation of diesel engine speed with the exhaust gas temperature

Fig. 6, shows the variation between the C.O.P and evaporator temperature when the generator temperature $T_g = 95\text{ }^\circ\text{C}$ and condenser temperature $T_c = 40\text{ }^\circ\text{C}$. The performance of evaporator is increased by increasing the temperature from $5\text{ }^\circ\text{C}$ to $15\text{ }^\circ\text{C}$ this is because of increment in latent heat of vaporization of the evaporator liquid fluid.

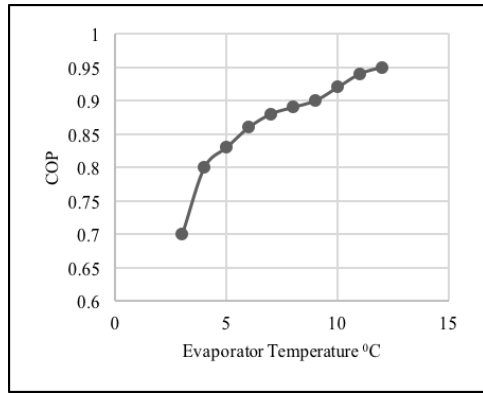


Fig. 6: Variation of COP with evaporator temperature

It has been shown from Fig. 7 that the heat of generator increases with increasing the exhaust gas temperature. As equation 2 shows, the higher the value of Q_g lower the value of C.O.P of air conditioning system.

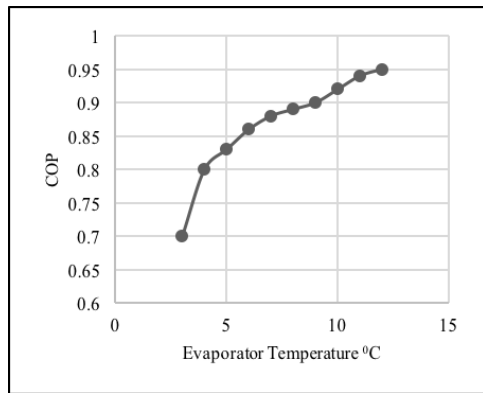


Fig. 7: Variation of exhaust gas temperature with heat generation Q_g

The trend of variation between the C.O.P and condensing temperature is shown in Fig. 8. It is clear from the characteristics of the condenser the greater the temperature of the condenser the more will be the heat rejected through it in the surrounding and this would be responsible to increase the net heat gain in the evaporator. It should be noted that the capacity of the evaporator is constant during the experiment.

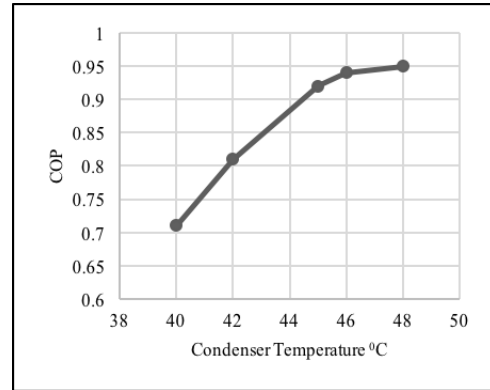


Fig. 8: Variation of COP with condenser temperature

Fig. 9 shows the variation of heat generated with C.O.P of the air-conditioning system that at constant heat capacity of the evaporator the performance of the system is higher at lower value of generator heat and moderate engine speeds.

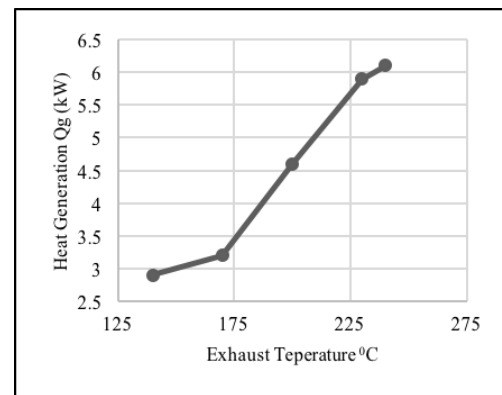


Fig. 9: Variation of COP with heat generation Q_g

6. Conclusions

Space air-conditioning system using waste energy from diesel gen set has been carried out in this investigation. The C.O.P highly depends on the working conditions of absorber, generator, condenser, and evaporator temperature. The ammonia absorption for space air-conditioning is an economically better concept for using exhaust gas heat. In this system the input comes from the exhaust gases, and very small amount of electric energy is used to operate the mechanical pump. Therefore it is advantageous to use the exhaust gas heat to operate space air conditioner for cooling purpose. The low performance of the system having poor economic advantage. This system can be an alternative of vapor compression system. With low maintenance, low level of noise and high reliability

system can be utilized commercially for space air conditioning.

References

- [1]. "The world Fact book-Saudi Arabia" (<https://www.cia.gov/library/publications/the-world-factbook/geos/sa.html>) Cia.gov. Retrieved 2011-04-28
- [2]. Saudi Aramco History (<http://www.saudiaramco.org>)
- [3]. <http://www.simmonsco-intl.com/files/Kuwait%20Talk.pdf>
- [4]. House, Karen Elliott (2012). On Saudi Arabia: Its People, past, Religion, Fault Lines and Future. Knopf. p. 245.
- [5]. Ministry of Water and Electricity – SAMIRAD (Saudi Arabia Market Information Resource)" (<http://www.saudinf.com/main/c6x.htm>). Saudinf.com. 2009-04-20. Retrieved 2011-04-28
- [6]. Energy Information Agency, Country Analysis Briefs 2007". (<http://www.eia.gov/>) Eia.doe.gov. Retrieved 2011-04-28.
- [7]. World carbon dioxide emissions data by country: China speeds ahead of the rest (<http://www.theguardian.com/news/datablog/2011/jan/31/world-carbon-dioxide-emissions-country-data-co2>) Guardian 31 January 2011
- [8]. Robert A, Frosch. Automotive absorption air conditioner utilizing solar and motor waste heat, United States Patent; 1980, 4,307,575.
- [9]. Bin Gadhi S, Agrawal R , and Kaushik. Computer aided analysis and thermal design of a signal effect absorption unit using Methanol-LiBr.ZnBr₂ mixture. Proceedings of the International Conference on Refrigeration and Air Conditioning, (Amman – Jordan); 1988, p.25-30.
- [10]. Frank F, Nekola, Trenton F. Heat generator for use with an absorption air conditioning system for Automobiles 1990; United State Patent, 5: 49-82.
- [11]. Alhusein M, Inayatullah. Automobile vapor absorption air conditioning system, J of Mu'tah for Research and studies 1994; 9:.251-269.
- [12]. Gui-ping Lin Xiu-gan Yuan Zhi-guang Mei, The feasibility study of the waste heat air-conditioning system for automobile, J of Thermal Science 1994; 3:2,
- [13]. Masadeh. S. Design and performance of automobile aqua-ammonia A/C System utilizing exhaust waste heat. Master Thesis, University of Jordan; 2002.
- [14]. Al-Aqeeli N, Gandhidasan P. The use of an open cycle absorption system in automobile as an alternative to CFC. The 6th Saudi Engineering Conference, KFUPM, Dhahran, December 2002; Vol. 5. P. 517-530.
- [15]. Shah Alam A. Proposed model for utilizing exhaust heat to run automobile air-conditioner, International Conference on "Sustainable Energy and Environment, 21-23 November 2006, Bangkok, Thailand.
- [16]. Silva CM, Costa .M and. Farias. Evaluation of SI engine exhausts gas emissions upstream and downstream of the catalytic converter, J Energy Conversion and Management 2006; 47: 2811–2828.
- [17]. Crepinsek Z, Goricanec D, Krope J. Comparison of the performances of absorption refrigeration cycles. J of WSEAS Transaction on Heat and Mass Transfer 2009; 3:65-76.
- [18]. Koehler J, Tegethoff WJ, Westphalen D, Sonnekalb M. Absorption refrigeration system for mobile applications utilizing exhaust gases. J Heat and Mass Transfer 1997; 32: 333–340.
- [19]. Holman JP. Heat Transfer, 9th ed. New York: McGraw-Hill; 2002.
- [20]. Mc Queiston C, Jerald P. Heating, Ventilating, and Air conditioning Analysis & Design. 4th ed. John Wiley & Sons, New York; 1997
- [21]. <http://www.eia.doe.gov/emeu/cabs/Saudi.html>

Synthesis, Characterization and Efficiency of Alum Produced from Waste Aluminium Cans for Wastewater Treatment

A.L. Adejumo

Department of Chemical Sciences, Osun State University, Osogbo, Osun state, Nigeria.
ayoade.adejumo@uniosun.edu.ng

R.U. Owolabi

Department of Chemical and Petroleum Engineering, University of Lagos, Akoka, Yaba, Lagos State, Nigeria.
uthmanrash642@yahoo.com

S.A. Adebisi

Department of Chemical Sciences, Osun State University, Osogbo, Osun state, Nigeria.
segun.adebisi@uniosun.edu.ng

W.A. Agbaje

Department of Chemical Sciences, Osun State University, Osogbo, Osun state, Nigeria.
agbajewb@yahoo.com

M.A. Usman

Department of Chemical and Petroleum Engineering, University of Lagos, Akoka, Yaba, Nigeria.
mawwal04@yahoo.com

Abstract

Herein, the synthesis, characterization and efficiency test of alum obtained from waste aluminium cans were investigated for wastewater treatment. Prior to the synthesis of the alum, the cans were subjected to physical treatments such as comminution (size reduction), plastic components removal, colour label removal, cleaning, pulverization etc. The physically treated waste aluminium cans were later chemically and step wisely converted to alum-a viable double salt. The process economy was found to be 99.37%. The synthesized alum and purchased alum were analyzed both qualitatively and quantitatively. The two samples exhibit similar coagulation performance.

Keywords: Alum; comminution; process economy; coagulation performance

1. Introduction

Aluminum is one of the most important metals used by modern societies. The combination of the physical properties of aluminium results in its use in a wide variety of products, many of which are indispensable to modern life. Partly to this reason, the global production of aluminium in 2005 rose to 31.9 million tonnes, and the world aluminum consumption, which was 45.3 Mt in 2006, is estimated to be 59 Mt in 2015, 92 Mt in 2020, and 120 Mt in 2025 (Menzie et al., 2010). For instance aluminium has a light weight, high corrosion resistance, good formability, and is non-toxic. These qualities have made aluminium the fastest-growing metallic material in the past 100 years (Boin, 2005). Aluminium has found application in transportation, packaging and construction company (EAA, 2012), household use, alloy (World coin news, 1992 and Skachkov, 2014). For the sake of brevity, the detailed chemistry of the aluminium can be found in most basic inorganic chemistry books and related publications.

Nonetheless, aluminium is found in combined state in over 270 different minerals (Ugwekar et al., 2012). The chief ore being bauxite (Al_2O_3) requires 780 kJ for the production of 1 mole of aluminium (Shakhashir, 2008). This amount is on a high side in terms of energy requirement and on a debit side in terms of cost for a product that will be eventually be discarded as waste even indiscriminately most of the time. For instance, with a global primary metal use of 27.4 million tonnes, a recycled aluminum production from purchased and tolled scrap of approximately 13.1 million tonnes in 2003, aluminium has taken the top position of all the non-ferrous metals (Boin, 2005). Though, recycling of aluminum saves considerable energy (26 kJ/mol) (Shakhashir, 2008) of aluminium but considering, the huge amount of aluminium to be recycled, this option seems energy and cost consuming in a country with a developing economy. Another viable option is to convert the waste aluminium into other aluminium compounds such as alum ($KAl(SO_4)_2 \cdot 12H_2O$), an important and common double

salt while simultaneously producing hydrogen gas.

Alum is a widely used chemical in industry, playing an important role in the production of many products used in the home and industry. The pulp and paper industry alone consumes 70 % of more than one million tonnes of alum produced annually in the United State of America. The second largest use is in the purification of water for human and industrial consumption (Ugwekar et al., 2012; Rice, 1957). Other uses include soaps, greases, fire extinguisher compounds, textiles, leather, synthetic rubber, drugs, cosmetics, cement, plastics, and pickles (Birni-Yauri, 2014). Alum's anti-perspirant and anti-bacterial properties (Ugwekar et al., 2012 and Aguilar et al., 1956) contribute to its traditional use as an underarm deodorant. Other uses of alum include its waterproofing agent and accelerator in concrete, as a clarifier for fats and oils and as a foaming agent in fire foams (Kanlayavattanukul et al., 2011), and finally, alum is the major adjuvant used to increase the efficacy of vaccines, and has been used since the 1920s (Mbow et al., 2011; Marrack et al., 2009). Alum has also been found to stop bleeding in cases of hemorrhagic cystitis (Kennedy, 1984). Hydrogen gas on the other hand has a great potential use as a fuel. Limited reports have been found on the synthesis of alum- a vital product from waste aluminium using local and cheap resources. In this report however, the aim is to synthesize a common aluminium compound called alum from aluminium waste to complement the existing waste aluminium waste management processes and also to make alum more readily available to the growing water treatment industries.

Recent product synthesis studies have shown the importance of process economy in the justification of such synthesis especially on a large scale basis (David et al., 2006). A number of metrics have been proposed almost a decade ago to make chemist's aware of the need to change the practice of chemical synthesis so that they become less wasteful, (David et al., 2006). Hudlicky et al., 1999 proposed a metric known as effective mass yield (Eq. 1.0) that is defined as the percentage of the mass of desired product relative to the mass of all non-benign materials used in its synthesis.

$$\text{Effective mass yield} = \frac{\text{mass of product}}{\text{mass of non-benign reagent}} \times 100 \quad (1)$$

Sheldon 1992 also proposed a metric known as E-factor which is defined as:

$$E \text{ factor} = \frac{\text{Total waste (kg)}}{\text{kg product}} \quad (2)$$

Curzons et al., 2001 similarly proposed a metric known as

$$\text{Mass Intensity} = \frac{\text{Total mass used in a process or process step (kg)}}{\text{mass of product (kg)}} \quad (3)$$

Other metrics (Eq. 4-5) developed and explored by GlaxoSmithKline both in U.S.A and U.K are

$$\text{Reaction Mass Efficiency} = \frac{\text{mass of product}}{\text{mass of reactant}} \times 100 \quad (4)$$

$$\text{Atom Economy} = \frac{\text{molecular weight of desired product}}{\text{molecular weights of all the reactants or products}} \quad (5)$$

Wang et al., (2011) also described and proposed another concept called real atom economy or effective atom economy (Eq. 6).

$$\text{Real Atom Economy} = \frac{\text{Actual weight of desired product (kg)}}{\text{Total weight of all raw materials in the product (kg)}} \quad (6)$$

Secondly, and to the best of our knowledge, no study has reported prior to this, the characterization or parameterization of the process economy of the aluminium waste management process the case of which is being considered in this study.

2. Materials and Reagents

Aluminium beverage cans were collected from domestic homes in Olorunkemi area, Oke-baale, Osogbo, Osun State, Nigeria longitude and latitude 7.7667° N, 4.5667° E, Distilled water, KOH, H₂SO₄, NaCl, BaCl₂, glycerol were obtained from Zayo-Sigma (Germany) while C₂H₅OH, HCl, isopropane and NH_{3(aq)} were obtained from Sigma-Aldrich (USA). All reagents were used as received.

2.1 Methods

2.1.1. Synthesis of Alum

The recent method of Birni-Yauri 2014 was adopted herein for the synthesis of the alum. Empty aluminium beverage cans were broken into small pieces. Plastic coatings over the cans were removed using sand paper. 1.0 g of clean aluminium pieces was weighed and transferred into 250 ml beaker and placed in a fume cupboard. 50 ml of 1.4 M KOH solution was slowly added till there is evidence of effervescence.

During the reaction, the initially colourless mixture was turned to dark grey and black. The cold black solution formed was filtered. The filtrate was a clear and colourless solution. The clear filtrate was transferred into a clean beaker, cooled by placing the beaker in a cooling bath of cold water. Slowly and carefully, (with a graduated cylinder) and stirring quickly with care, 20.0 mL of 9.0 M solution of H_2SO_4 was added to the cooled and colourless solution till the solution get warm. Initially, a thick, white, gelatinous precipitate was formed, as more acid was added. The solution was boiled to evaporate excess water. The final solution contains potassium ions (K^+), (from potassium hydroxide KOH used), aluminium ion (Al^{3+}), and sulfate ions (SO_4^{2-}). Reaction beaker was kept into the ice-water bath to chill. The mixture was allowed to chill for 15 minutes, and as the solution cools, solid alum precipitated out forming alum crystals. Finally, the alum crystal was removed from the solution after 24 hours by filtration and washed with a mixture of 20 % v/v aqueous ethanol i.e. 20 ml of absolute ethanol and with 20 ml of water in a 50 ml graduated cylinder. This serves to wash the isolated crystal as it dries. The crystal was placed on filter paper and allowed to dry overnight and then re-weighed. The synthesized alum crystal was analyzed against purchased alum.

2.2 Qualitative Analysis

The following basic qualitative analyses were carried out on the synthesized Alum crystal.

2.2.1. Analysis for sulphate ion (SO_4^{2-}) in the synthesized alum crystal

1.5 g of the dried Alum crystals was pulverized. A spatula tip full of the pulverized alum powder was added into a test tube filled half way with distilled water and the solution was stirred with a stirring rod until dissolution is complete. Two drops of aqueous barium chloride ($BaCl_2$) solution was added to the mixture. A white precipitate formed, which was insoluble indicated the presence of sulfate ion (SO_4^{2-}) in the synthesized alum crystals.

2.2.2. Analysis for Potassium ion (K^+) in the synthesized alum crystal

Flame test was used to test for the presence of potassium ion in the synthesized alum. The crystal was

held in the flame for 20 seconds until the solid glows. Potassium was volatilized and red flame turned to pale purple flame which indicates the presence of potassium ion (K^+) in the synthesized alum crystals.

2.2.3. Analysis for Aluminium ion (Al^{3+}) in the synthesized alum crystal

The method of Birnin-yuri and Musa (2014) was adopted for the analysis of aluminium ion in the synthesized alum crystal. Two drops of diluted 1.4M KOH was added to the dissolved alum solution. Sulfuric acid (H_2SO_4) in drop and in excess was also added to the alum solution. A thick, white gelatinous precipitate was formed, insoluble in drop but soluble in excess which indicates the presence of aluminium ion (Al^{3+}) in the synthesized alum crystals.

2.2.4. Melting Point of the synthesized alum crystal

0.5g of dry pulverized alum was packed into a melting point capillary tube. The tube was fastened to a thermometer. The alum was leveled with the bulb of the thermometer and a universal clamp and cork stopper was used to fasten the thermometer to a ring stand. The bottom of the capillary tube and thermometer was immersed in the beaker of water and heated. The water was stirred to maintain an even distribution of temperature.

2.3 Quantitative analysis

The following quantitative analyses were carried out on the ions present in the synthesized alum crystal using flame photometry and Atomic Absorption Spectroscopy (AAS) respectively.

2.3.1. Analysis for Potassium ion (K^+) in the synthesized alum crystal Using Flame Photometry.

0.5 g of alum sample was dissolved in distilled water in 50 ml volumetric flask. Few drops of concentrated hydrochloric acid was added. A blank and potassium calibration standards was prepared in stepped amount in a reasonable ranges. Emission intensity was determined at 766.5 nm. Calibration curve was constructed from the potassium standards. Potassium concentration of sample was determined from the calibration curve.

2.3.2. Analysis for Sulfate ion (SO_4^{2-}) in the Synthesized Alum crystal using Atomic Absorption spectroscopy (AAS)

0.5 g of alum sample was dissolved in 50 ml distilled water. 2.0 ml of the diluted sample was then added to 1.0 ml of conditioning reagent. Standard solution was prepared at 5.0 mg/L sulphate range. The absorbance measurements were mark on spectrophotometer at wavelength of 425.0 nm and it was used to prepare calibration curve.

2.4 Coagulation Analysis

2.4.1. Acidity /Alkalinity and colour of the synthesized alum

The pH meter electrodes were immersed in the water sample and equilibrium was established between electrodes and sample by stirring sample to ensure homogeneity. Thereafter, the pH was read and recorded. The colour was determined by visual comparison of the sample.

2.4.2. Turbidity

Turbidometer was used for sampling a well mixed sample and the readings were taken. Results from nephelometric measurements are expressed as nephelometric turbidity units (NTU)

2.4.3. Total Solids

20.0 ml of a well-mixed alum sample was evaporated in a weighed dish and dried to constant weight in an oven at 105 °C for 24 hours. It was then cooled in a desiccator, weighed and recorded. The total solids are expressed as:

$$\text{Total Solids, mg/L} = \frac{(W_2 - W_1) \times 1000}{\text{Sample volume, ml}}$$

where:

W_1 = Weight of dish, mg and

W_2 = Weight of dried residue + dish, mg

2.4.4. Total Dissolved Solids

20.0 ml of a well-mixed sample was filtered under vacuum through a standard glass fiber filter, and the filtrate was evaporated to dryness in a weighed dish and dried to constant weight at 180 °C for 1 hour. It was then cooled in a desiccator, weighed and recorded. The drying was repeated until a constant weight is obtained.

The total dissolved solid is expressed as:

$$\text{Total Filterable Residue, mg/L} = \frac{(A - B) \times 1000}{C}$$

Where:

A = Weight of dried residue + dish

B = Weight of dish

C = mL of filtrate used

2.4.5. Total Suspended Solids

20.0 ml of a well-mixed sample was filtered through a weighed standard glass-fiber filter. The residue retained on the filter paper was dried to a constant weight at 103 to 105 °C. The increase in weight of the filter represents the total suspended solids. To obtain an estimate of total suspended solids, the difference between the total dissolved solids and total solids was calculated. Therefore total suspended solids can be calculated thus:

$$\text{Total Suspended Solids, mg/L} = \frac{(A - B) \times 1000}{\text{ml sample}}$$

where:

A = Weight of filter + dried residue, mg, and

B = Weight of filter, mg.

3. Results and Discussion

The qualitative analysis of the synthesized alum crystal is reported in Table 1. The potassium, aluminium and sulphate ions were positively tested as expected. The purchased alum similarly responded positively to the same qualitative analyses.

Quantitative analysis were carried out on the synthesized crystal to know the amount of each ions present in the crystal. The results of both the synthesized alum crystal and purchased alum crystal are shown in Table 2. Flame photometry and Atomic absorption spectroscopy (AAS) were used respectively to quantify the ions present in both the synthesized solid crystal and the purchased alum crystal. The result of the analysis shows that the synthesized solid crystal contained potassium and sulphate with concentration (ppm) 1524.930 ± 0.016 and 16.581 ± 0.000 and the purchased alum crystal contained potassium and sulphate with concentration (ppm) $1518.050 \pm$

0.017 and 12.571 ± 0.000 . In general, it is observed that quantitative analysis of the synthesized solid crystal contain both potassium and sulphate and the concentration (ppm) are in close range with that of the original purchased alum. Potassium and sulphate ions in the synthesized alum crystal were higher compared to the purchased alum. This may be due to the presence of potassium hydroxide (KOH) and sulphuric acid H_2SO_4 used in synthesizing the alum crystal.

Table 1: Qualitative analysis of ions present in the synthesized alum crystal

Test	Observation	Inference
Alum solution + Aqueous $BaCl_2$ Solution	White Precipitate formed, and insoluble (After 20 hours)	SO_4^{2-} Confirmed
Solid Alum Crystal + heat (10 minutes)	Red flame turned to lavender (pale purple) flame color	K^+ Confirmed
Aluminate ion Solution + $H_2SO_4(aq)$ in drop and in Excess	Thick, white gelatinous precipitate formed insoluble in drop but soluble in excess	Al^{3+} Confirmed

Table 2: Quantitative analysis of ions present in synthesized and purchased Alum crystal.

Ions	Conc. (ppm) Mean \pm SD	Method
K^+	^a 1524.930 / ^b 1518.050	Flame photometry
SO_4^{2-}	^a 16.581 / ^b 12.571	AAS

^a Synthesized alum crystal ^b Purchased alum crystal

Coagulation Performance

The effectiveness of the two alum samples (i.e. synthesized and the purchased one) was carried out. An initial experiment was performed to determine the initial characteristics of the raw wastewater for monitoring the effectiveness of the alum samples. 1.0 g each of alum crystal was applied to the waste water for coagulation purpose. The characteristics of the wastewater with purchased and synthesized alum before and after coagulation are summarized in Table 3. The appearance of the wastewater was initially muddy but after coagulation it became clear and colourless, and the wastewater was also very turbid initially but after coagulating with the synthesized alum it became less turbid. It can also be observed that

the synthesized alum crystal performed slightly more coagulation action than that of purchased alum crystal. The summary of calculated values is shown in Table 4.

Table 3: Result for test of Coagulation action of synthesized and Purchased Alum crystal

Parameters	Test tube A (Before Coagulation)	Test tube B (After coagulation)
Volume of wastewater (ml)	^{a,b} 20.00	^{a,b} 20.00
pH of muddy water	^{a,b} 11.76	^a 4.47 / ^b 4.88
Appearance of water	^{a,b} muddy	^{a,b} clear and colourless
Turbidity (NTU)	^{a,b} 1.58	^a 2.92 / ^b 2.98
Total solids (mg)	^{a,b} 2.50	^{a,b} 1.50
Total dissolved solids (mg)	^{a,b} 4.00	^{a,b} 2.00
Total suspended solids (mg)	^{a,b} 1.50	^{a,b} 0.50

^a Synthesized alum crystal ^b Purchased alum crystal

Table 4: Summary of calculated values

Parameter	Calculated value
Melting point of Alum	$^{\circ}C$ 92
Mass of Alum obtained	10.020 g
Number of mole of Aluminium used	0.0434 mol
Number of mole of Alum	0.680 mol
Theoretical yield of Alum	322.592 g
Percentage yield of Alum	3.161%
Number of mole of water of crystallization	12.255
Mass Conc. (ppm) of SO_4^{2-}	16.581 ± 0.000
Mass Conc. (ppm) of K	1524.930 ± 0.016

The above parameters were calculated to know the mass of synthesized alum obtained from the chemical process, theoretical yield of alum and the percentage yield of the alum. The following values were calculated in other to know the effectiveness of these chemical

recovery methods. The melting point of the synthesized alum crystal is 92 °C. The chemical recovery method is thereby found to be effective and efficient because 1.17g of aluminium can was used to produce 10.020g of alum. Similarly the atom economy of the process has been found through eq. (5) as 99.37%.

4. Conclusion

The synthesis of alum from aluminum related waste is feasible. Apart from ridding the environment off discarded items, demands of the growing water treating industries is also being met. The synthesis is therefore a better waste aluminium management practice. Similarly, it has a high atom economy which is a current trend in the green and sustainable chemistry. The economical feasibility of the process is outside the scope of the present study and therefore recommended for future studies.

References

- Aguilar, T. N., Blaug, S.M. and Zopf, L.C., 1956. A study of the antibacterial activity of some complex aluminum salts, *Journal of the American Pharmaceutical Association*, 45, pp. 498–500.
- Birin-Yauri, A.U. and Musa, A., 2014. Synthesis and Analysis of Potassium Aluminium Sulphate (Alum) from Waste Aluminium Can, *International Journal of Advanced Research in Chemical Science*, 1, pp. 1-6.
- Boin, U.M.J. and Bertram, M., 2005. Melting Standardized Aluminum Scrap: A Mass Balance Model for Europe, overview, 2005.
- Curzons, A.D, Constable, D.J.C. Mortimer and Cunningham, V. L., 2001. *Green Chemistry*, 3, pp. 1–6.
- David J. C. C, Alan D. C and Virginia L. C., 2002. Metrics to ‘green’ chemistry—which are the best? *Green Chemistry*, 4, pp. 521–527.
- Etuaful, R.K. Production of Alum from Bauxite Waste from Awaso mine, 2013. M.Sc Thesis, Kwame Nkrumah University of Science and Technology, Ghana.
- European Aluminium Association (EAA), 2012. Sustainability of Aluminium in Buildings Retrieved 13 October, 2015.
- Hetherington, L. E., 2007. World Mineral Production. British Geological Survey, ISBN 978-0-85272-592-4.
- Hudlicky, T., Frey, D.A., Koroniak, L., Claeboe, C.D., Brammer, L.E., 1999. *Green Chemistry*, pp. 57–59.
- Kanlayavattanukul, M. and Lourith, N., 2011. “Body malodours and their topical treatment agents”. *International Journal of Cosmetic Science*, 33, pp. 298–311.
- Kennedy, C., Snell, M.E. and Witherow, R.E., 1984. Use of Alum to Control Intractable Vesical Haemorrhage, *British Journal of Urology*, 56, pp. 673–675.
- Marrack, P., McKee, A. S. and Munks, M.W., 2009. Towards an understanding of the adjuvant action of aluminium, *Nature Reviews Immunology*, 9, pp. 282–7.
- Mbow, M L. De Gregorio, E., and Ulmer, J. B., 2011. Alum’s adjuvant action: grease is the word, *Nature Medicine*, 17, pp. 415–416.
- Menzie, W.D., Barry, J.J, Bleiwas, D.I., Bray, E.L., Goonan, T.G. and Matos, G., 2010. The Global Flow of Aluminum from 2006 through 2025.
- Rice, J. K., 1975. The use of organic flocculants and flocculating aids in the treatment of industrial water and industrial waste water, *Symposium on Industrial Water and Industrial Waste Water (ASTM International)*, 207, pp. 41–51.
- Skachkov, V. M., Pasechnik, L. A., Yatsenko, S.P., 2014. Introduction of scandium, zirconium and hafnium into aluminum alloys. Dispersion hardening of intermetallic compounds with nanodimensional particles, *Nanosystems: physics, chemistry, mathematics*, 5, pp. 4.
- Shakhashiri, B. Z., 2008. Chemical of the Week: Aluminum SciFun.org. University of Wisconsin, Retrieved 13 October 2015.
- Sheldon R A. E., 2008. Factors, green chemistry and catalysis: an odyssey, *Chemical Communications*, 29, pp. 3352–3365.
- Sheldon, R.A. (1992). *Chemical Industry*, London, 903–906..
- Ugwekar R.P. and Lakhawat, G.P., 2012. Potash Alum from Waste and Medicinal Foil, 2012. *IOSR Journal of Engineering*, 2, pp. 62-64.
- Wang, W., Lu, J., Zhang, L, and Li, Z., 2011. Real atom economy and its application for evaluation the green degree of a process, *Frontiers of Chemical Science and Engineering*, 5, pp. 349-354.
- Whitten, K. W., Davis, R. E., and Peck, L., 1996. *General Chemistry*, 5th Ed., Saunders College Publishing, Philadelphia.
- World Coin News (WCN), (1992. World’s coinage uses 24 chemical elements, Part 1.
- World Coin News (WCN), 1992. World’s coinage uses 24 chemical elements, Part 2.

Concomitant Administration of Quercetin and α -tocopherol Protects Rats from Cadmium Chloride Induced Neural Apoptosis and Cognitive Dysfunction

Ali A. Shati

Biology Department, College of Science, King Khalid University, Abha, Saudi Arabia,
aaalshati@kku.edu.sa

Abstract

Cadmium (Cd), a highly toxic environmental pollutant, leads to a neurotoxicity and cognitive dysfunction in both animals and humans. In spite of the available in vitro evidence, there is a paucity of literature on the mechanisms by which CdCl₂ induced these effects, in vivo. While numerous in vivo studies have shown a protective effect of Quercetin (QUR) against neurodegenerative disease, there is still uncertainty about the safety of such efficiency of QUR due to its low bioavailability. Therefore, trails to enhance this have shown increased brain accumulation of QUR when administered in conjugation with α -tocopherol. Consequently, this study aimed to investigate the molecular effects of individual and combined administration of QUR and α -tocopherol against CdCl₂ induced apoptosis and memory loss in rats. Results of the current study revealed that CdCl₂ induced neural apoptosis, spatial memory loss and disturbed brain cholinergic system in mechanisms related to increased oxidative stress, inhibition of protein phosphatase (PP2A) induced activation of ERK1/2 and JNK and activation of PTEN induced inhibition of Akt/mTOR/S6K1 signaling pathways. As compared to individual effects of QUR or α -tocopherol which were not effective to ameliorate CdCl₂ induced apoptosis and cognitive dysfunction, combined administration of both drugs in both control and CdCl₂ intoxicated rats could significantly enhance levels of antioxidant defense, improved cognitive dysfunction by enhancing levels of acetylcholine (Ach) and protein levels of CREB and BDNF, and decreased neural apoptosis by upregulating levels of PP2A induced inhibition of ERK1/2 and JNK signaling as well as downregulating expression of PTEN induced activation of Akt/mTOR/S6K1 signaling. In conclusion, only concomitant administration of QUR and α -tocopherol but not their individual use, provide an excellent protective formula against CdCl₂ induced neurodegeneration and memory loss.

Keywords: ERK1/2; JNK; Akt/m-TOR; Quercetin; α -tocopherol; apoptosis; cognitive dysfunction

1. Introduction

Cadmium (Cd) induced neurotoxicity is characterized by neurotransmitters levels alterations (Lafuente et al., 2000; Pari and Murugavel, 2007), metabolic changes (Lafuente, and Esquifino, 1999; Lafuente et al., 2000); behavioral and memory disturbance (Wright et al., 2006; Mendez-Armenta and Rios, 2007) and neurodegeneration (Mendez-Armenta and Rios, 2007; Chen et al., 2008).

Currently, there is a growing recognition that neuronal cell death characteristic of Cd-induced neurodegeneration and its associated cognitive dysfunction are partially but highly related to increased apoptosis. In this regard, in vitro evidence using neurons cultures has shown that such effect is mediated by over-production of reactive oxygen species (ROS) induced activation of two members of mitogen-activated protein kinase (MAPK) signaling, namely, c-Jun N-terminal kinase (JNK) and extracellular signal-regulated kinase 1/2 (Erk1/2) (Chen et al. 2008, Chen et al., 2011a). Moreover, using the same in

vitro model, Cd-induced-neuronal apoptosis was also partially mediated by an unexpected activation of the mammalian target of rapamycin (mTOR) signaling pathway (Chen et al. 2008, Chen et al., 2011a; Chen et al., 2011b, Chen et al., 2014). On the other hand, the flavonoid, Quercetin (QUR), is a well reported neuroprotective agent in rodents that acts by inhibiting apoptotic cell death, preventing neurotransmitter disturbance and enhancing cognitive dysfunction in various animal models of neuronal injury and neurodegenerative diseases induced experimentally (Zhang et al., 2015, Xia et al., 2015) or induced by toxic metals such as lead (HU et al., 2008), methyl mercury (Barcelos et al., 2011), tungsten (Sachdeva et al., 2015) and Cd (Unsal et al., 2015).

The neuroprotective effect of QUR has been referred to its antioxidant and anti-apoptotic effects as well as its ability to activate sirtuins (SIRT1) induced autophagy (Yokoo and Kitamura, 1997; Costa et al., 2016). QUR inhibits apoptosis by inhibiting the activities of both JNK and ERK-1 in mesangial cells, fibroblasts, and epithelial cells (Yokoo and Kitamura,

1997; Ishikawa et al., 1997; Uchida et al., 1999). In spite of this, there is still uncertainty about the safety and efficiency of QUR administration on neural function in both animals and human. This has been raised as QUR could induce cell death through the inhibition of Akt/PKB and ERK survival pathways in cultured neurons (Spencer et al., 2003).

Further criticism of the neuroprotective effect of QUR has been raised later as only very low concentrations have been detected in the brain of the animals, after oral or intraperitoneal administration (from pmol to nmol) (de-Boer et al., 2005; Ishisaka et al., 2011) which was shown to be due to the extensive intestinal and hepatic metabolism of QUR (Shirai et al., 2006). Hence, several trails to increase QUR bioavailability have confirmed accumulative concentrations in the brain of animal when administered in conjugation with α -tocopherol (Ferri et al., 2015). Of interest is also the observation that conjugated QUR is less metabolized and can enter the red blood cells where it is converted to its non-conjugated form being transported to various tissue (Fiorani et al., 2003).

However, the regulatory effect of QUR on various members of MAPKs and Akt/mTOR cell signaling in the brain of rats intoxicated with Cd is completely lacking. In addition, given the fact that co-administration of QUR with α -tocopherol enhances its blood-brain barrier (BBB) transport and the fact that QUR is still debated regarding its neural safety, this study aimed to investigate the molecular effects of administration of QUR alone or in combination with α -tocopherol on memory function, cholinergic neurotransmitters levels, and neural survival and apoptotic pathways in control rats and in rats intoxicated with cadmium chloride (CdCl_2). The latter aim was achieved by examining the cortical activities of ERK1/2, JNK, P38 and Akt/mTOR signaling pathways.

2. Materials and Methods

2.1 Animals

The study was conducted at the animal house of the College of Science, King Khalid University, Abha, Saudi Arabia, according to the guidelines for the care and use of laboratory animals set by the institution which follow the regulations of laboratory animal care and use, published by the US National Institutes of Health (NIH publication No. 85-23, revised 1996). A total of fifty-six young adult male Wistar albino rats 5 weeks old, weighing 100–105 g were used in this study. Rats were randomly divided into seven groups (n=8/group). Each group was housed in a separate

cage in a constant temperature (22–24°C) and light-controlled room on an alternating 12:12 h light-dark cycle and had free access to food and water. Rats were fed a standard commercial pellet diet and were kept for one week before beginning the experiment for acclimatization.

2.2 Experimental Protocol

Cadmium chloride CdCl_2 and Quercetin (QUR, Empirical Formula: $\text{C}_{15}\text{H}_{10}\text{O}_7$) were purchased from Sigma-Aldrich (St. Louis, MO) and were always prepared freshly by dissolving in normal saline. Rats groups (n=8/group) were subjected to treatment as follows:

Group 1 (Control group): Rats received distilled water (5 ml/kg .b.w. and 0.1ml of coconut oil), orally.

Group 2 (CdCl_2 intoxicated group): Rats received CdCl_2 (5 mg/kg.b.w.), orally.

Group 3 (QUR treated group): Rats received QUR (15 mg/kg.b.w.), intraperitoneally.

Group 4 (α -tocopherol treated group): Rats received a dose of 120 IU α -tocopherol diluted in 0.1 ml of coconut oil, orally.

Group 5 (QUR+ α -tocopherol treated group): Rats received QUR (15mg/kg.b.w.), i.p. and received a concomitant dose of 120 IU α -tocopherol diluted in 0.1 ml of coconut oil, orally.

Group 6 (Cd+Qur treated group): Rats orally received CdCl_2 (5 mg/kg.b.w.) and received a concomitant dose of QUR (15 mg/kg.b.w.), intraperitoneally.

Group 7 (Cd+Qur+ α -tocopherol treated group): Rats orally received CdCl_2 (5 mg/kg.b.w.) and received concomitant doses of QUR (15 mg/kg.b.w.), intraperitoneally and treated with 120 IU α -tocopherol diluted in 0.1 ml of coconut oil, orally.

All treatments were carried out on daily basis for four consecutive weeks (30 days). Dose selections and routes of administrations of all drugs were based on previous studies that showed a neurotoxic effect of CdCl_2 at this dose (Shagirtha et al., 2011) and showed a neuroprotection effect of QUR (Unsal et al., 2013) and neurological safe dose of α -tocopherol (Guimarães et al., 2015).

2.3 Assessment of cognitive performance

Spatial learning and memory were assessed using the Morris Water Maze (MWM) as previously described by Sethi et al. (2008). MWM consists of a black 168cm diameter circular pool divided into 4 equal hypothetical quadrants and filled with water (50 cm deep, temperature 20 ± 2 °C). An escape circular platform was submerged at 2 cm below the surface of the water. The principle of the test is to train the rats to escape from swimming by climbing onto the visible platform and over time the rats apparently learn the spatial location of the platform from any starting position at the circumference of the pool. During the test, each rat of any group was placed inside the water tank at 4 different entry quadrant points and was given 4 trials/day (90 sec/trial) for 4 consecutive days, starting from day 31 to day 34 following the end of all treatments. Escape latency (sec) was recorded to determine changes in learning dysfunction. The animal was allowed to swim for 60 sec to find the hidden platform. If failed, then it was manually guided to the platform. At the end of each trial, each rat was allowed to remain on the platform for 30 seconds. MWM training was recorded by a web camera attached to the laboratory ceiling.

2.4 Collection of brains and homogenates preparation

After the MWM test, rats were anesthetized with sodium pentobarbital (60-70 mg/kg, i.p.) their brains were quickly removed on ice, washed with cold saline and immediately replaced in ice-cold dishes. Parts of brain tissues (100mg) were homogenized individually in either 9 volumes cold 50 mM Tris buffer (pH 7.4) or in 0.5 ml RIPA buffer (150 mM sodium chloride 1.0% NP-40 or Triton X-100 0.5% sodium deoxycholate 0.1% SDS, 50 mM Tris, pH 8.0). Protease inhibitors (Cat. No. P8340, Sigma-Aldrich, St. Louis, MO, USA) and phosphatase (PhosSTOP, Cat. No. PHOSS-RO Sigma-Aldrich, St. Louis, MO, USA) were added to these buffers according to manufacturer's instructions to prevent protein degradation and auto-phosphorylation. Supernatants collected were used from these homogenates were used for biochemical assays and western blot studies, respectively. However, other parts of the brain were stored in liquid nitrogen for further use.

2.5 Determination of oxidative stress markers in the brain homogenates

Malondialdehyde (MDA) levels as Lipid peroxidation markers were measured as levels of Thiobarbituric acid reactive substances (TBARS)

using a commercial assay kit (Cat No. NWK-MDA01, NWLSS, USA). Reduced glutathione (GSH) concentrations were measured using an assay kit (Cat. No. 703002, Cayman Chemical, Ann Arbor, MI, USA). Superoxide dismutase (SOD) activities were measured using a commercial kit (Cat. No. 706002, Cayman Chemical, Ann Arbor, MI, USA). Glutathione peroxidase (GPx) activities were measured using a commercial kit (Cat. No. 703102, Cayman Chemical). All tests were done according to the manufacturer's instruction.

2.6 Assay of cholinergic markers

The cholinergic markers were measured in the brain homogenates of all rats using commercially available kits. The content of choline acetyltransferase (ChAT) was determined using ELIZA commercial available kit (Cat. No SEB929Ra, Cloud-Clone Corp. Houston-TX, USA). Colorimetric commercially available kits were used to determine the content of Acetylcholine (Ach, Cat. No. Cell Biolabs, Inc, STA-603, San Deigo, CA-USA) and the activity of Acetylcholine esterase (AChE, CAT. No. ab138871, abcam, UK). All tests were done according to the manufacturer's instruction and were run in triplicates.

2.7 Western blot analysis

Protein concentrations in the supernatants collected from homogenization of brain tissues in RIPA buffer were measured by Bradford assay and then were separated using 10% SDS-PAGE (60 µg protein/well). Membranes were incubated for 10 minutes at room temperature in blocking buffer (5% milk in 1X TBST buffer). Then, the membranes were then washed 3X with 1X TBST buffer (10 minutes each) followed by incubation with the desired primary antibody for 2 hours. After washing again with 3X with 1X TBST buffer, the membranes were incubated for another 2 hours with horseradish peroxidase-conjugated secondary antibody. All incubations with the antibodies were done in a rotator shaker and all dilution was minimized for each antibody. Bound antibodies intensities were evaluated using a Pierce-enhanced chemiluminescence (ECL) kit (Thermofisher, USA, Piscataway, NJ). Images were scanned using C-DiGit Blot Scanner (LI-COR, USA) with the supplied Image Studio DiGits software. Protein expressions were presented as relative expressions to that of β -actin. Monoclonal or polyclonal antibodies against ERK1/2 (p44-42 MAPK, Cat # number 9102, 42,44 kDa), p-ERK1/2 (p-p44-42 MAP, Thr202/Tyr204, Cat # number 9101, 42.44 kDa), p-BAD (ser 112, Cat # number 9291, 23 kDa), mTOR (Cat # number #2972, 289), phospho-mTOR (Ser2448,

Cat # 2971, 289 kDa), c-Jun (Cat # 9165, 43.48 kDa), phospho-c-Jun (Ser63, Cat # 9261, 48 kDa), Akt (Cat # 9272, 60 kDa), phospho-Akt (Thr308, Cat # 9275, 60 kDa), and p-70S6K (Cat # 9202, 70.85 kDa), pp-70S6K (Thr389, Cat # 9205, 70.85 kDa), PP5 (Cat # 2289, 58 kDa) and cleaved caspase 3 (Asp175, Cat # 9661, 17/19 kDa) were purchased from Cell Signaling Technology, USA. Antibodies against PP2A α (Cat #, ab137825, 36 kDa) and p-BAD (ser 184) (Cat # ab216829, 18 kDa) were purchased from Abcam (UK). Antibodies against PTEN (Cat #, A2B1 sc-7974, 55 kDa); were purchased from Santa Cruz Biotechnology Inc., CA, USA, 36 kDa).

2.8 Statistical Analysis

Graphpad prism statistical software package (version 6) was used to perform all statistical analysis and generating figures. In Morris Water Maze (WMT), Comparisons between the rats within the same groups or within the groups were performed using one-way analysis of variance (ANOVA) with repeated measure or one-way ANOVA on rank, respectively followed by Tukey's test for multiple comparisons. All other data were analyzed using one-way ANOVA followed by Tukey's test. Differences were considered significant if $p < 0.05$. Data are presented as mean \pm SD.

3. Results

3.1. Mortality rate

Although, the experimental procedure started with 8 rats, 3 deaths were found in group 2 administered with CdCl₂ and no mortality was detected in any of the other groups during the experimental procedure. Therefore, the mortality rate due to CdCl₂ intoxication was 37.5%. Hence, it could be speculated that QUR or α -tocopherol administration alone or in conjugation increased survival rate to 100% in CdCl₂ intoxicated rats. However, the 3 dead rats in the CdCl₂ intoxicated group were replaced by other 3 rats to make the total number for each group is eight.

3.2. Assessment of cognitive and memory dysfunction

Assessment of cognitive dysfunction in rats was achieved by analysis of Morris water maze (MWM) (Fig. 1), measuring levels of brain cholinergic markers (Fig. 2) and protein levels of CREB and BDNF (Fig. 8), two markers related to memory and synaptic plasticity. In MWM, escape latencies (time needed to find a visible submerge platform) of 4 trails/day/rat were analyzed and compared within and between the groups over periods of consecutive 4 days performed at the end of all treatments. While individual administration

of QUR or α -tocopherol to control rats has no effect on all of the above-mentioned parameters, concomitant administration of both drugs significantly shortened the escape latencies for test days 3 and 4, enhanced levels of Ach and activities AChT as well as protein levels CREB and PDNF and significantly lowered activities of AChE, in respect to control rats. On the other hand, increased average escaped latencies over all days of memory assessment with significantly decreased levels of Ach, CREB and BDNF and activities of AChT and significantly enhanced levels of ACHE were seen in CdCl₂ intoxicated rats received the vehicle or QUR alone as compared control rats, results that were not significantly different within or between both groups. However, Concomitant administration of QUR and α -tocopherol to CdCl₂ intoxicated rats significantly decrease the average escape latencies and significantly alleviated the levels of Ach, CREB, BDNF and activities of AChE, AChT to normal levels seen in the control rats, as compared to CdCl₂ model rats. The resulted latencies in this group of rats were not significantly different to their corresponding latencies observed in the control rats overall testing days.

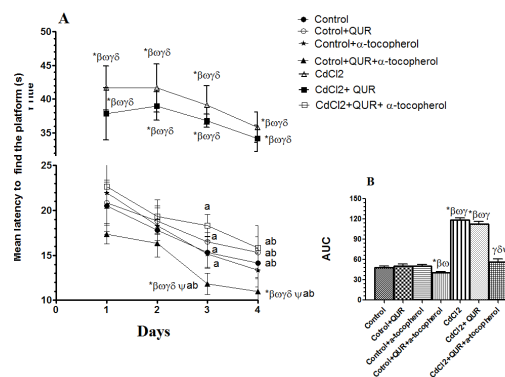


Fig. 1: Average mean latency to find hidden platform in water maze test (MWM, A) and area under the curve (B) in all groups of rats. Each data point represents the mean \pm SD latency of the 4 trials/rat/day for a total of 8 rats/group. a: significantly different when compared to day 1 within the same group. b: significantly different when compared to day 2 within the same group. *: versus control, β : versus Control+QUR. ω : versus control + α -tocopherol. δ : versus Control+QUR + α -tocopherol. δ : significantly different as compared to CdCl₂. Ψ : Significantly different as compared to CdCl₂+QUR.

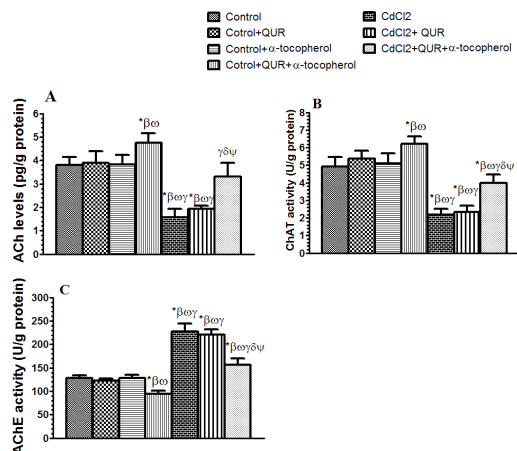


Fig. 2: Levels of Acetylcholine (ACh, A), Acetylcholine transferase (AChT, B) and Acetylcholine esterase (AChE, C) in the brain homogenates of all rat groups. Values are presented as mean \pm SD of 8 rats/group. *: versus control, β : versus Control+QUR. ω : versus Control+ α -tocopherol. : versus Control+QUR+ α -tocopherol. δ : significantly different as compared to CdCl₂. Ψ : Significantly different as compared to CdCl₂+QUR

3.3. Oxidative stress evaluation:

Biochemical analyses of oxidative stress markers are depicted in Fig. 3. Data revealed that individual administration of QUR or α -tocopherol to control rats has no effect on brain levels of MDA and GSH or activities of SOD and GPx, as compared to control rats received the vehicle. However, combined administration of QUR or α -tocopherol to control rats significantly lowered MDA levels and significantly raised GSH levels and activities of SOD and GPx in the brain of these control rats as compared to control rats received the vehicle. On the other hand, CdCl₂ intoxication resulted in significant decreases in the levels of GSH and activities of SOD and GPx and significantly increased levels of MDA in the brain tissue of intoxicated rats, levels that was partially but significantly improved by individual QUR therapy. However, when conjugated together, QUR and α -tocopherol resulted in further significant increases in the levels of GSH and activities of SOD and GPx and significantly lowered the MDA as compared to CdCl₂ model groups received the vehicle or QUR.

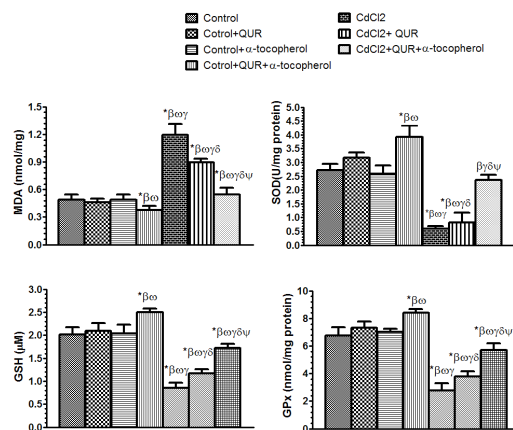


Fig. 3: Levels of Malondialdehyde (MDA) and reduced glutathione (GSH) and activities of superoxide dismutase (SOD) and glutathione peroxidase (GPx) in brain homogenates of all rat groups. *: versus control, β : versus Control+QUR. ω : versus Control+ α -tocopherol. : versus Control+QUR+ α -tocopherol. δ : significantly different as compared to CdCl₂. Ψ : Significantly different as compared to CdCl₂+QUR.

3.4. Effects on mitogen-activated protein kinase signal (MAPK) signaling:

Phosphorylated and total protein levels components of ERK1/2 signaling pathway including (MAPK 54/56 (ERK1/2), p-ERK1/2, BAD and p-BAD (Ser 112) and JNK signaling pathway including (JNK, p JNK, c-Jun, p-c-Jun and p-BAD (Ser128) in the brain tissue of all groups of rats were investigated (Fig. 4 and Fig. 5). Moreover, as MAPK activity is regulation by kinase and phosphatases, the levels of their upstream regulators namely protein phosphatase 2A and 5 (PP2A and 5, respectively) were also investigated (Fig. 8). While increased P-BAD (Ser 112) is known to be anti-apoptotic, enhanced level of p-BAD (Ser 128) is apoptotic. To confirm these effects levels of cleaved caspase-3 in the brain tissues were also measured (Fig. 6). Total levels of all the tested proteins were always stable in the brain tissue of all groups of rats. In the control groups of rats, solely QUR or α -tocopherol CdCl₂ intoxication didn't affect phosphorylation levels of all of the above-mentioned proteins neither levels of cleaved caspase-3, PP2A or PP5. CdCl₂ administration to rats significantly activated both ERK 1/ and JNK signaling and activated intrinsic apoptosis 2 as indicated by upregulation of p-ERK1/2, p-JNK, p-c-Jun, decreased levels of p-BAD (Ser 112) and increased levels of p-BAD (Ser128) and cleaved caspase-3, as compared to control rats. In this regards, CdCl₂ intoxication significantly lower levels of PP2A but not PP5 in the brain tissues of these rats.

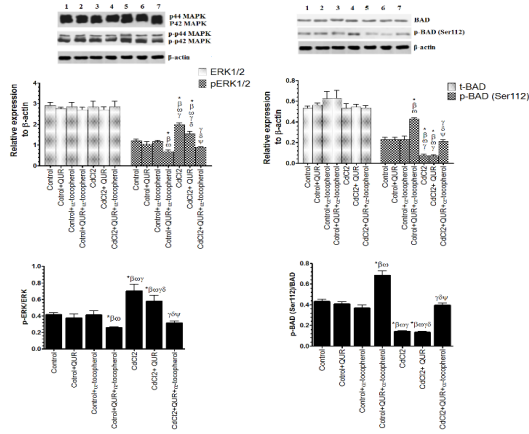


Fig. 4: Protein levels of total extracellular signal-regulated kinase 1/2 (Erk1/2), p-ERK1/2 (Thr202/Tyr204), total BAD and p-BAD (Ser 112) in the brain tissues of all rat groups as detected by western blot. *: versus control (1), β: versus Control+QUR (2). ω: versus Control+α-tocopherol (3). ϖ: versus Control+QUR+α-tocopherol (4). δ: significantly different as compared to CdCl₂ (5). Ψ: Significantly different as compared to CdCl₂+QUR. 7: CdCl₂+QUR+α-tocopherol

On the other hand, However, combined administration of QUR and α-tocopherol to control rats significantly downregulated ERK1/2 and JNK signaling as indicated by the significant decreases in the levels of p-ERK1/2, p-JNK and p-c-JUN and enhanced levels of PP2A. Interestingly, associated with these changes, both drugs significantly increased levels of p-BAD (Ser 112) and significantly decreased levels of p-BAD (Ser128) and cleaved caspase 3. Such effects were also partially achieved by individual QUR administration and further significantly increased toward their normal levels in the brain of CdCl₂ intoxicated rats when QUR and α-tocopherol were administered in conjugation, as compared to CdCl₂ intoxicated rats received the vehicle.

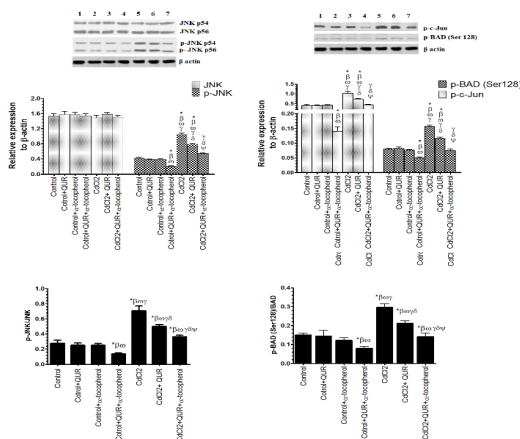


Fig. 5: Protein levels of the total c-Jun N-terminal kinase (JNK), p-JNK (Thr183/Tyr185), p-c-Jun (Ser63) and p-BAD (Ser128) in the brain tissues of all groups of rats as detected by

western blot. *: versus control (1), β: versus Control+QUR (2). ω: versus Control+α-tocopherol (3). ϖ: versus Control+QUR+α-tocopherol (4). δ: significantly different as compared to CdCl₂ (5). Ψ: Significantly different as compared to CdCl₂+QUR. 7: CdCl₂+QUR+α-tocopherol.

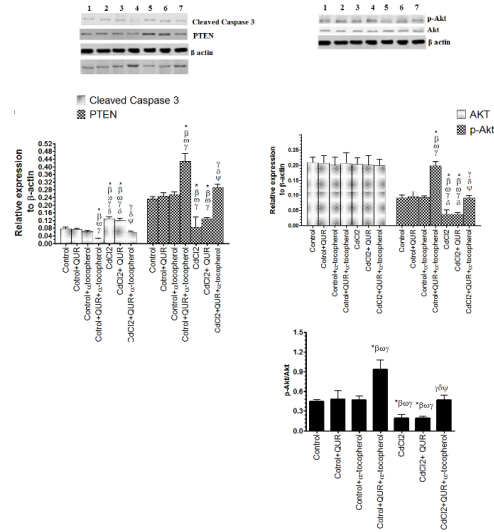


Fig. 6: Protein levels of Cleaved caspase 3, PTEN, Akt and p-Akt (Thr308) in the brain tissues of all groups of rats as detected by western blot. *: versus control (1), β: versus Control+QUR (2). ω: versus Control+α-tocopherol (3). ϖ: versus Control+QUR+α-tocopherol (4). δ: significantly different as compared to CdCl₂ (5). Ψ: Significantly different as compared to CdCl₂+QUR. 7: CdCl₂+QUR+α-tocopherol

3.5. Effects on mammalian target of rapamycin (mTOR) signaling

The levels of phosphorylation and total protein levels of the signaling pathway Akt/mTOR/S6K1 and the levels of its negative regulator PTEN were studied in the brain tissue of all groups of rats (Fig. 6 and Fig. 7). Of interest, individual QUR administration tended to increase the activity of Akt but significantly increased levels of p-mTOR and its downstream targets, p-S6K1 without affecting the expression of PTEN. However, when QUR was administered concomitantly with α-tocopherol, it significantly lowered levels of PTEN and raised protein levels of p-Akt, p-mTOR and p-S6K1 as compared to all other control groups. CdCl₂ intoxication significantly inhibited this signaling pathway as indicated by the significant decreases in the levels of p-Akt, p-mTOR and p-S6K1 and significant increases in the levels of PTEN. On the other hand and unlike to situation in the control group, individual administration of QUR to CdCl₂ intoxicated rats failed to regulate expression levels of all of this protein and only significant downregulation of PTEN and

upregulation of p-Akt, p-mTOR and p-S6K1 levels were seen when it was administered in conjunction with α -tocopherol, all levels of which were not significantly different as compared to control rats.

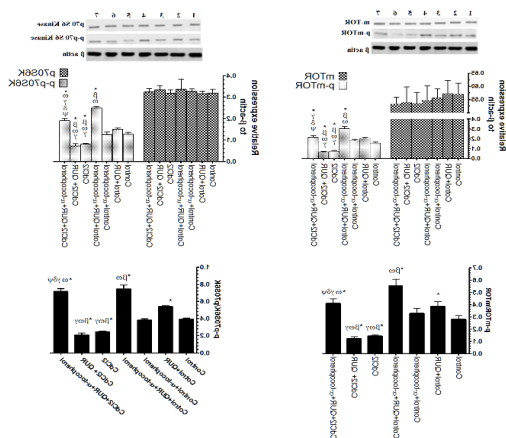


Fig. 7: Protein levels of mammalian target of rapamycin (m-TOR), p-mTOR (Ser2448), p70S6K and p-p70S6K (Thr389) in the brain tissues of all groups of rats as detected by western blot. *: versus control (1), β: versus Control+QUR (2). ω: versus Control+ α -tocopherol (3). δ: significantly different as compared to CdCl₂ (5). Ψ: Significantly different as compared to CdCl₂+QUR. 7: CdCl₂+QUR+ α -tocopherol.

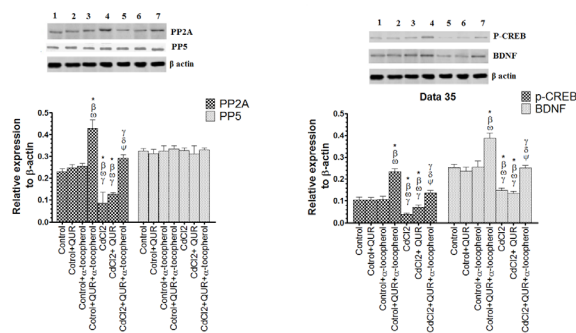


Fig. 8: Protein levels of protein phosphatase 2A (PP2A), protein phosphatase 5 (PP5), cAMP-responsive element-binding (p-CREB) and brain-derived neurotrophic factor (BDNF) in the brain tissues of all groups of rats as detected by western blot. *: versus control (1), β: versus Control+QUR (2). ω: versus Control+ α -tocopherol (3). δ: significantly different as compared to CdCl₂ (5). Ψ: Significantly different as compared to CdCl₂+QUR. 7: CdCl₂+QUR+ α -tocopherol.

4. Discussion

The aim of the current study was to investigate the effect of QUR alone or in conjunction with administered α -tocopherol on neural apoptosis and

associated cognitive dysfunction and in rats which are either control or intoxicated with CdCl₂, in vivo and to investigate the molecular mechanisms behind this protection. The major finding of the current study are 1) CdCl₂ activated neural apoptosis and induced neurotransmitters disturbance and spatial memory loss. 2) These effects were associated with enhanced oxidative stress and inhibition of protein phosphatases 2A (PP2A) induced activation of ERK1/2 and JNK as well as with activation of PTEN induced inhibiting of Akt/mTOR signaling. 3) In both control and CdCl₂ intoxicated rats, QUR and only when administered in conjunction with α -tocopherol, enhanced spatial memory function, and reduced markers of apoptosis by activating Akt/mTOR survival pathway and downregulated the ERK1/2 and JNK apoptotic pathways, an effect that is associated with decreased neural oxidative stress.

The mechanism by which CdCl₂ induces neural oxidative stress induced neural damage, apoptosis and its own enhanced permeability across the blood brain barrier (BBB) of adult brains appears to be mediated by disruption of the prooxidant/antioxidant balance. This is achieved indirectly by replacing iron and copper ion from a number of cytoplasmic and membrane proteins, activating Fenton reaction and (Casalino et al. 1997) and depletion of selenium-induced reduced glutathione (GSH) levels and GSH peroxidase (GPx) activities (Lopez et al., 2006; Chen et al., 2014). In support to this, enhanced levels of Malondialdehyde (MDA), reduced levels of GSH as well as activities of total superoxide dismutase (SOD) and GPx have been detected in the brains of rats intoxicated with CdCl₂. However, in control rats, QUR tended to lower MDA levels and enhance the antioxidant systems with a more profound when it was administered as a conjugate with α -tocopherol, suggesting to act as a prooxidant rather than antioxidants to stimulate the cell's own antioxidant defense mechanisms as has been previously suggested (Halliwell, 2008; Halliwell, 2013).

In comparison to its partial antioxidant ameliorative effect in CdCl₂-intoxicated rats when administered alone, QUR completely restored the activities of these antioxidant enzymes and GSH levels when it was administered in conjunction with α -tocopherol even look similar, the finding does not support the findings reported by Unsal et al. (2003) who have shown that QUR completely ameliorated levels of MDA and activities of SOD in the brain of rats intoxicated with CdCl₂. This could be explained by the expected low levels (nanomolar) of QUR in the brain tissue upon solely QUR administration (Ishisaka et al., 2011). In support, it has been reported that at least

millimolar levels of any antioxidant (i.e glutathione and vitamin C) are required to scavenge free radicals in the brain tissue (Schaffer and Halliwell, 2012).

On the other hand, cell apoptosis is a well control mechanism that includes many cell signaling pathways. Among all, MAPKs (ERK1/2, JNK and P38) and PI3K/Akt/mTOR play many roles under pathological intoxication with CdCl₂ (Chen et al., 2008, Chen et al., 2013). In most tissues and Erk1/2 and PI3K/Akt/mTOR were shown be survival pathways, whereas JNK and p38 signaling cascades have been shown to promote neuronal cell death (Detta et al., 1997; Davis 2000; Lei and Davis , 2003; Rockwell et al., 2004; Shimamura et al., 2000).

In the neural cortical tissues, while JNK activation phosphorylates BAD at Serine128 (Ser128) to promotes its apoptotic effect (Donovan et al., 2002), both ERK1/2 and Akt induce phosphorylation of Bad at Ser136 (Ser136) and/or Serine112 (Ser112) to inhibit apoptosis (Detta et al., 1997; Shimamura et al., 2000). However, even it is a survival signal, ROS-induced sustained activation of ERK1/2 initiates either intrinsic or extrinsic apoptosis in vitro and in vivo (Cagnol and Chambard, 2010).

Using cultured neurons, ROS induced by CdCl₂ activated all members of MAPK family including ERK1/2, JNK, and p38 by direct inhibition of serine/threonine protein phosphatases 2A (PP2A) and protein phosphatase 5 (PP5). In the same line, orally administered CdCl₂ to rats upregulated both ERK1/2 and JNK, an effect that was mediated at least by inhibition of PP2A but not PP5, as evident by the detected cellular protein levels. Interestingly, p-BAD (Ser 128) significantly increased whereas p-BAD (ser 112) significantly decreased, suggesting that both ERK1/2 and JNK activations are pro-apoptotic. However, in contrast to in vitro studies of Chen et al. (2011a; 2011b; 2014) who have shown that CdCl₂ activated PI3K/Akt/mTOR induced apoptosis on culture neurons by inhibiting PTEN, the current in vivo model shows that administration of CdCl₂ inhibited Akt/ mTOR survival pathway through activating PTEN, suggesting a decreased activity of this survival pathway.

Neither QUR nor α -tocopherol solely administration affected any protein levels involved in all these signaling pathways in both control and Cd-intoxicated rats. Interestingly, conjugation of both drugs together significantly enhanced levels of PP2A resulting in significant inhibition of both ERK1/2 and JNK signaling with a concomitant inhibition of PTEN

mediated activation of Akt/mTOR/S6K1 signaling in the brains of control rats or CdCl₂-intoxicated rats. Associated with these effect enhanced levels of p-BAD (Ser 112) and decrease levels of pBAD (Ser 128) with a parallel decrease in cleaved caspase 3 were seen, suggesting a neurosurvival effect of QUR, only if administered with α -tocopherol under both control or CdCl₂-intoxication conditions.

In parallel to the enhanced oxidative stress, a decrease in cognitive dysfunction with parallel decreases in the levels of acetylcholine (Ach)and choline acyltransferase (ChAT) activity and increase in acetylcholinesterase (AChE) activity were seen in the brain tissues of CdCl₂-intoxicated rats. These effect were only ameliorated in the group of rats only administered QUR in conjugation with α -tocopherol.

Although previous reports have shown decreased levels of Ach in the brain of rat after CdCl₂ intoxication (Desi et al., 1988) and are positively correlated with enhanced oxidative stress (Ahmad et al., 2012; Xi et al., 2014; Lafuente et al., 2000; Pari and Murugavel, 2007), this study enriches the available literature and shows that CdCl₂ induced cognitive dysfunction is also associated with lower brain protein levels of p-CREB and its downstream target, BDNF, both of which play roles in neuronal proliferation, synapse remodelling, synaptic plasticity and memory function (Finkbeiner et al., 1997; Mizuno et al., 2002). However, large number of intracellular signal transduction pathways converge CREB and regulate CREB activity (Carlezon et al., 2005). In CNS, activation of numerous signaling pathways are known to upregulate CREB levels. These include PKB/Akt, MAPKs, and calcium-calmodulin kinase IV (CaMKIV) (Barco et al., 2003; Carlezon et al., 2005). In accordance with the available evidences, it can be conclude that CdCl₂ affects the spatial memory in rats by inhibiting Akt signaling pathway and that conjugation of QUR and α -tocopherol rather than their individual doses are able to enhance the levels of CREB and PDNF by activation of this pathway. In support, a flavonoid extracted from blueberry induced activation of CREB and BDNF expression has also been shown to lead to the activation of the PI3K/Akt/mTOR signaling pathway (Williams et al., 2008).

Despite the current evidences, this study still has some limitations. For instance, the doses of QUR used here was based on many previous studies in literature that showed a neuroprotective effect of QUR at this dose. Hence, future work should investigate the effect of QUR alone in this animal model at higher doses to compare the effects and confirm the main findings of the current study. Furthermore, results presented in

this study showed that the effect of QUR on cognitive function and biochemical alterations related to this effect in whole brain. As the hippocampus is one of the important brain structure affected in neurodegenerative diseases, further investigation on these molecular pathways at the level of the hippocampus would be advantageous and will clearly add much more support to the current findings. Finally, it is highly recommended to repeat this study on other species (e.g. mice and rabbits) and on the same species of another sex or aged rats.

5. Conclusion

This study clearly demonstrates neither QUR nor α -tocopherol alone are able to rescue the neurons and enhance special memory against CdCl₂ induced neurotoxicity. However, when both drugs are administered in conjugation, are able to reduce cell apoptosis and enhance spatial memory in CdCl₂ intoxicated rats by activated PP2A induced inhibition of ERK1/2 and JNK apoptotic pathways and by inhibiting PTEN induced activation of Akt/mTOR/S6K1 survival pathway.

Acknowledgements

The author would like to thank technical staff at Department of biology and the staff of the animal house at King Khalid University for their technical help in the current study.

Conflicts of Interest

The author has no conflict of interest and the work was not supported or funded by any company.

References

Ahmad, A., Khan, MM., Javed, H., Raza, SS., Ishrat, T., Khan, MB., Safhi, MM., Islam, F., 2012. Edaravone ameliorates oxidative stress associated cholinergic dysfunction and limits apoptotic response following focal cerebral ischemia in rat. *Mol. Cell. Biochem.* 367 (1-2): 215–225.

Barcelos, G., Grotto, D., Serpeloni J., Angeli J., Rocha B., de Oliveira Souza V., Vicentini J., Emanuelli T., Bastos J.K., Antunes L., Knasmüller S., Barbosa F., 2011. Protective properties of quercetin against DNA damage and oxidative stress induced by methylmercury in rats. *Archives of Toxicology* 85 (9), pp 1151–1157.

Barco, A., Pittenger, C., Kandel, ER., 2003. CREB, memory enhancement and the treatment of memory disorders: promises, pitfalls and prospects. *Expert. Opin. Ther. Targets* 7(1):101–114.

Cagnol, S., Chambard, J., 2010. ERK and cell death: Mechanisms of ERK-induced cell. Death, apoptosis, autophagy and senescence. *FEBS Journal* 277 (1), pp 2–21.

Carlezon, W., Duman, R., Nestler, E., 2005. The many faces of

CREB. *Trends Neurosci.* 28(8), pp436–445.

Casalino, E., Sblano, C., Landriscina, C., 1997. Enzyme activity alteration by cadmium administration to rats: the possibility of iron involvement in lipid peroxidation. *Archives of Biochemistry and Biophysics* 346 (2), pp171–179.

Chen, L., Liu, L., Huang, S., 2008. Cadmium activates the mitogen-activated protein kinase (MAPK) pathway via induction of reactive oxygen species and inhibition of protein phosphatases 2A and 5. *Free Radical Biology and Medicine* 45 (7), pp1035–1044.

Chen L., Xu B., Liu L., Luo Y., Zhou H., Chen W., Shen T., Han X., Kontos C.D. & Huang S. 2011b. Cadmium induction of reactive oxygen species activates the mTOR pathway, leading to neuronal cell death. *Free Radic. Biol. Med.* 50 (5), pp624–632.

Chen S., Xu Y., Xu B., Guo M., Zhang Z., Liu L., Ma H., Chen Z., Luo Y., Huang S. & Chen L. 2011a. CaMKII is involved in cadmium activation of MAPK and mTOR pathways leading to neuronal cell death. *J. Neurochem.* 119 (5), pp1108–1118.

Chen, S., Ren, Q., Zhang, J., Ye, Y., Zhang, Z., Xu, Y., Guo, M., Ji, H., Xu, C., Gu, C., 2014. N-acetyl-L-cysteine protects against cadmium-induced neuronal apoptosis by inhibiting ROS-dependent activation of Akt/mTOR pathway in mouse brain. *Neuropathology and Applied Neurobiology* 40 (6), pp759–77.

Cořta, L., Garrick, J., Roquè, P., Pellacani, C., 2016. Mechanisms of Neuroprotection by Quercetin: Counteracting Oxidative Stress and More. *Oxidative Medicine and Cellular Longevity* 2016.

Davis, R., 2000. Signal transduction by the JNK group of MAP kinases. *Cell* 103 (3), pp 239–252.

de Boer, VCJ., Dihal, AA., vander-Arts, I.C., Wolfram, S., Alink, GM., Rietjens, IM., Keijer, J., Hollman, PC., 2005. Tissue distribution of quercetin in rats and pigs. *The Journal of Nutrition.* 135 (7), pp 1718–1725.

Detta, SR., Dudek, H., Tao, X., Masters, S., Fu, H., Gotoh, Y., Greenberg ME. 1997. Akt phosphorylation of BAD couples survival signals to the cell-intrinsic death machinery. *Cell*, pp 91 (2): 231–41.

Desi, I., Nagymajtenyi, L., Schulz, H., 1998. Behavioural and neurotoxicological changes caused by cadmium treatment of rats during development. *Journal of Applied Toxicology* 18(1), pp 63–70.

Donovan, N., Becker, E., Konishi, Y., Bonni, A., 2002. JNK phosphorylation and activation of BAD couples the stress-activated signaling pathway to the cell death machinery. *The Journal of Biological Chemistry* 277 (43), pp40944–40949.

Ferri, P., Angelino, D., Gennari, L., Benedetti, S., Ambrogini, P., Del Grande, P., Ninfali, P., 2015. Enhancement of flavonoid ability to cross the blood–brain barrier of rats by coadministration with α -tocopherol. *Food & Function* 6 (2), pp 394–400.

Finkbeiner, S., Tavazoie, SF., Maloratsky, A., Jacobs, KM., Harris, KM., Greenberg ME. 1997. CREB: a major mediator of neuronal neurotrophin responses. *Neuron* 19 (5): 1031–1047.

Fiorani, M., Accorsi, A., Cantoni, O., 2003. Human red blood cells as a natural flavonoid reservoir. *Free Radical Research* 37(12), pp 1331–1338.

Guimarães, M., Murad, L., Paganelli, A., de Oliveira, C., Vianna, L., 2015. Effects of alpha-tocopherol associated with lovastatin on brain tissue and memory function in SHRSPs. *Physiology & Behavior* 149 (1), pp 303–309.

Hu, P., Wang, M., Chen, W., Chen, L., Yin, S., Yong, W., Chen, J., Wang, H., Ruan, D., 2008. Quercetin relieves chronic lead

- exposure-induced impairment of synaptic plasticity in rat dentate gyrus in vivo. *Naunyn-Schmiedeberg's Archives of Pharmacology* 378(1), pp 43–51.
- Halliwell, B., 2008. Are polyphenols antioxidants or pro-oxidants? What do we learn from cell culture and in vivo studies? *Archives of Biochemistry and Biophysics* 476 (2), pp 107–112.
- Halliwell, B., 2013. The antioxidant paradox: less paradoxical now?. *Br. J. Clin. Pharmacol.* 75(3), pp 637–644.
- Ishikawa, Y., Yokoo, T., Kitamura, M., 1997. c-Jun/AP-1, but not NF- κ B, is a mediator for oxidant-initiated apoptosis in glomerular mesangial cells. *Biophys Res. Commun.* 240 (2), pp 496–501.
- Ishisaka, A., Ichikawa, S., Sakakibara, H., Piskula, M., Nakamura, T., Kato, Y., Ito, M., Miyamoto, K., Tsuji, A., Kawai, Y., Terao, J., 2011. Accumulation of orally administered quercetin in brain tissue and its antioxidative effects in rats. *Free Radical Biology and Medicine* 51(7), pp 1329–1336.
- Lafuente, A., Esquifino, I., 1999. Cadmium effects on hypothalamic activity and pituitary hormone secretion in the male. *Toxicology Letters* 110 (3), pp 209–18.
- Lafuente, A., Marquez, N., Pazo, D., Esquifino, A., 2000. Effects of subchronic alternating cadmium exposure on dopamine turnover and plasma levels of prolactin, GH and ACTH. *BioMetals* 13 (1), pp 47–55.
- Lei K., Davis R., 2003. NK phosphorylation of Bim-related members of the Bcl2 family induces Bax-dependent apoptosis. *Proc. Natl. Acad. Sci.* 100 (5), pp2432–2437.
- Lopez, E., Figueroa, S., Oset-Gasque, M., Gonzalez, M., 2003. Apoptosis and necrosis, pp Two distinct events induced by cadmium in cortical neurons in culture. *British Journal of Pharmacology* 138 (5), pp 901–911.
- Mendez-Armenta, M., Rios, C., 2007. Cadmium neurotoxicity. *Environmental Toxicology and Pharmacology* 23(3), pp 350–358.
- Mizuno, M., Yamada, K., Maekawa, N., Saito, K., Seishima, M., Nabeshima, T., 2002. CREB phosphorylation as a molecular marker of memory processing in the hippocampus for spatial learning. *Behav. Brain Research* 133(2), pp135–141.
- Pari, L., Murugavel, P., 2007. Diallyl tetrathiolane improves cadmium induced alterations of acetylcholinesterase, ATPases and oxidative stress in brain of rats. *Toxicology*. 234 (1-2), pp 44–50.
- Rockwell, P., Martinez, J., Papa, L., Gomes, E., 2004. Redox regulates COX-2 upregulation and cell death in the neuronal response to cadmium. *Cellular Signalling* 16 (3), pp343–353.
- Sachdeva, S., Pant, S., Kushwaha, P., Bhargava, R., Flora, S., 2015. Sodium tungstate induced neurological alterations in rat brain regions and their response to antioxidants. *Food and Chemical Toxicology* 82 (1), pp 64–71,
- Schaffer, S., Halliwell, B., 2012. Do polyphenols enter the brain and does it matter? Some theoretical and practical considerations. *Genes & Nutrition* 7 (2), pp 99–109.
- Sethi, P., Jyoti, A., Singh, R., Hussain, E., Sharma, D., 2008. Aluminium-induced electrophysiological, biochemical and cognitive modifications in the hippocampus of aging rats. *Neurotoxicology* 29 (6), pp1069–79.
- Shagirtha, K., Muthumani M., Milton Prabu S. 2011. Melatonin abrogates cadmium induced oxidative stress related neurotoxicity in rats. *European Review for Medical and Pharmacological Sciences* 15 (9), pp 1039–1050.
- Shirai, M., Kawai, Y., Yamanishi, R., Kinoshita, T., Chuman, H., Tera, J., 2006. Effect of a conjugated quercetin metabolite, quercetin 3-glucuronide, on lipid hydroperoxide-dependent formation of reactive oxygen species in differentiated PC-12 cells. *Free Radic Res.* 40(10), pp 1047–53.
- Shimamura, A., Ballif, B., Richards, S., Blenis, J., 2000. Rsk1 mediates a MEK–MAP kinase cell survival signal. *Current Biology* 10 (3), pp 127–135.
- Spencer, J., Rice-Evans, C., Williams, R., 2003. Modulation of pro-survival Akt/protein kinase B and ERK1/2 signaling cascades by quercetin and its in vivo metabolites underlie their action on neuronal viability. *Journal of Biological Chemistry* 278(37), pp 34783–93.
- Uchida, K., Shiraiishi, M., Naito, Y., Torii, Y., Nakamura, Y., Osawa, T., 1999. Activation of stress signaling pathways by the end product of lipid peroxidation. 4-hydroxy-2-nonenal is a potential inducer of intracellular peroxide production. *The Journal of Biological Chemistry* 274 (4), pp2234–2242.
- Unsal, C., Kanter, M., Aktas, C., Erbogaa, M., 2015. Role of quercetin in cadmium-induced oxidative stress, neuronal damage, and apoptosis in rats. *Toxicology & Industrial Health* 31(12), pp1106–1115.
- Williams, C., El Mohsen, M., Vauzour, D., 2008. Blueberry-induced changes in spatial working memory correlate with changes in hippocampal CREB phosphorylation and brain-derived neurotrophic factor (BDNF) levels. *Free Radical Biology and Medicine* 45(3), pp295–305.
- Wright, O., Amarasiriwardena, C., Woolf, A., Jim, R., Bellinger, D., 2006. Neuropsychological correlates of hair arsenic, manganese, and cadmium levels in school-age children residing near a hazardous waste site. *Neurotoxicology* 27 (2), pp210–216.
- Xia, S., Xie, Z., Qiao, Y., Li, L., Cheng, X., Tang, X., Shi, Y., Le, G., 2015. Differential effects of quercetin on hippocampus-dependent learning and memory in mice fed with different diets related with oxidative stress. *Physiology & Behavior* 138 (1), pp 325–331.
- Xi Y, Wang M., Zhang W., Bai M., Du Y., Zhang Z. Li Z. & Miao J2014. Neuronal damage, central cholinergic dysfunction and oxidative damage correlate with cognitive deficits in rats with chronic cerebral hypoperfusion. *Neurobiology of Learning and Memory* 109 (1), pp 7–19.
- Yokoo, T., Kitamura, M., 1997. Unexpected protection of glomerular mesangial cells from oxidant-triggered apoptosis by bioflavonoid quercetin. *The American Journal of Physiology* 273 (2 pt2), pp206–212.
- Zhang, Y., Yi, B., Ma, J., Zhang, L., Zhang, H., Yang, Y., Dai, Y., 2015. Promotes neuronal and behavioral recovery by suppressing inflammatory response and apoptosis in a rat model of intracerebral hemorrhage. *Neurochemical Research* 40 (1), pp 195–203.

Structural Investigation of Semi Crystalline LDPE Nano-polymer

M. S. Gaafar^{1,2}, H. Afifi²

¹College of Science, Physics. Department., Majmaah University., Zulfi, Kingdom of Saudi Arabia,

m.gaafar@mu.edu.sa

²National Institute for Standards, Ultrasonic Department, Giza, Egypt.

Kh. Al Zenidy

College of Science, Physics Department, Majmaah University, Zulfi, Kingdom of Saudi Arabia

Abstract

Low density polyethylene (LDPE) nano-polymers were subjected to a high power ultrasonic irradiation as a polymerization initiator, for different times (0, 5, 10 and 15 minutes). Characterization was performed on the non-irradiated and irradiated LDPE samples by measuring the low power ultrasonic wave velocities (Longitudinal and Shear) along with density measurements. X-ray diffraction (XRD) patterns revealed that the percentage crystallinity and crystalline size had changed significantly with exposure to ultrasonic irradiation. The XRD patterns showed, the usual peaks relative to the planes (110) and (200). The XRD parameters indicated the formation of LDPE nano-polymer and the increase in the degree of crystallinity, lattice constants (a & b) and crystallite size for nano-LDPE samples with exposure time from 0 to 10 min, while with exposure time up to 15 min they decreased. However, the results obtained by the X-ray diffraction have been confirmed by the ultrasonic wave velocities together with densities of the samples.

Keywords: LDPE; Ultrasonic wave velocities; X-ray; Ultrasonic viscosity

1. Introduction

Ultrasonic investigation of liquid mixtures consisting of polar and non-polar components is of considerable importance in understanding intermolecular interaction between the component molecules because they have diverse and important applications in several industrial and technological processes [1-3]. Moreover, this study also focuses on the behaviour of a non-polar molecule in a different polar environment. These liquid mixtures are of interest to organic chemists who want to know about the types of bonds, type of molecular interactions, etc. The values of ultrasonic velocity, density, viscosity and adiabatic compressibility as a function of concentration will be of much help in providing such information. Moreover, such studies are useful in gaining insight into the structure and bonding of associated molecular complexes and other molecular processes. The ultrasonic study can give the indication of complex formation through hydrogen bonding in the system. Recently researchers suggested that adiabatic compressibility also used for detecting hydrogen bond formation in solutions. The ultrasonic velocity measurement is a unique tool in characterizing the structure and properties of the system and provides significant information about the arrangement of matter in solutions. It also finds an extensive application in studying the nature of intermolecular forces. Accurate

knowledge of thermodynamic mixing properties such as adiabatic compressibility, intermolecular free length, free volume, internal pressure and molar volume and their excess values for mixtures of protic, non-protic and associated liquids has a great importance in theoretical and applied areas of research.

LDPE is a popularly used food stretch or shrinks wrap material owing to its versatile usability, affordability, and safety [4]. Also, polyethylene is the most widespread polymer in the world. It belongs to the family of the polyolefin. The annual production is approximately 80 million metric tons in 2008 [5]. Especially, low-density polyethylene is widely used in greenhouses as covering material due to its dielectric properties, durability [6], excellent chemical resistance [7-9], good resistance to cracking, low permeability to water vapor [10], low cost and easy manufacturing [6, 11].

The X-ray diffraction (XRD) and scanning electron microscopy (SEM) were used by M. Hamouya et al. [12] to study the natural ageing of low-density polyethylene greenhouses covering films. His study by XRD showed the presence of the peaks relative to the planes (110), (200) and (020) and the emergence of the new peak at the angular range of 43.50- 43.60° corresponding to the plane (220) with different time.

The preferential oxidation of the amorphous phase relative to the crystalline phase is a result of the higher diffusion of oxygen within it. The peaks around this latter phase are due to oxidation processes. The results obtained by the infrared have been confirmed by observing the morphology of the samples with scanning electron microscopy technology [12].

Characterization of polymeric materials has been carried out by means of thermodynamic, mechanical and spectroscopic methods [13-16]. The ultrasonic velocity and the elastic properties are of the most important factors determining the polymers properties; several experimental methods have been used to estimate the static and dynamic viscoelastic properties. Further parameters such as ultrasonic absorption, ultrasonic viscosity, adiabatic compressibility, acoustic impedance and Rao's constant can be calculated. These parameters are useful in understanding the nature of interactions of polymers. Several earlier papers have addressed these problems of polymers in single solution.

The food industry is increasingly aware of the importance of developing new analytical techniques to inspect the complex structures of food and to monitor online their properties during the production processes. The main reason for this increase arises from the fact that ultrasonic technologies are nondestructive, rapid and easy to automate. In addition, they can easily be adapted to analyze optically opaque systems and the cost has been reduced due to the new electronic technologies.

The ultrasonic wave propagation in real media is accompanied by several phenomena, among which we mention: absorption [17], diffraction [18], and non-linearity [19]. As the physicochemical properties change from one medium to another, the intensities of the phenomena mentioned above change as well [20]. Therefore, the measurement of acoustic parameters (e.g. absorption coefficient or velocity) in a given propagation medium is of great interest since it can be exploited to control the quality of some foodstuff products, especially fluid.

The aim of this work is to investigate the structure and properties of LDPE with ultrasonic irradiation.

2. Experimental Methods

The LDPE samples were prepared as liquids by mixing 5 g of LDPE, 0.25 g clay in 400 ml xylene. The mixture of every sample was heated to 80 °C. X-ray diffraction of the prepared samples was investigated by

x-ray diffraction using Brucker X-ray diffractometer. All diffraction patterns were recorded between $1 < 2\theta \leq 30^\circ$, the $\Delta\theta$ was 0.01° and time interval was 4 seconds.

The mixtures were subjected to high power ultrasonic irradiation using Branson sonifier (S-450D & 400W) at different irradiation times (0, 5, 10, 15 minutes). The high power ultrasonic irradiation technique, was used to break the polymer chains to nano sized polymer latex particles [21 - 23].

The ultrasonic velocities in the liquid mixtures were measured using pulse-echo method (USN 60 Flaw detector) and the Krautkramer transducer, operating at a frequency of 2MHz (central frequency of 0.7 MHz and bandwidth of 1.4 MHz) as shown in Fig. 1. The uncertainty of the measurements is 10 m/sec. Using an oscilloscope (60 MHz time base oscilloscope, Philips, Netherlands) direct measurement of the time required for the pulses to travel twice the length of the specimen is possible, to allow immediate calculation of the ultrasonic wave velocity as given in the following equation [21]:

$$V = 2L/\Delta t \quad (1)$$

where L is the liquid length and Δt is the time interval. The ultrasonic absorption coefficient (α) and ultrasonic viscosity (η_u) are given in the form;

$$\alpha = (20/2L) \log (A_n/A_{n+1}) \quad (2)$$

$$\eta_u = (\rho\alpha V^3)/(26.3f^3) \quad (3)$$

where A_n/A_{n+1} is the ratio between two successive echoes A_n , A_{n+1} , ρ is the density of the liquid and f is the ultrasonic frequency. The uncertainty of the measurements of ultrasonic absorption and viscosity are ± 0.01 dB/cm and ± 0.03 mPa.s respectively. The experimental measurements were performed for all examined liquid samples having varied densities at ambient temperature 25°C. Each experiment was repeated three times and through three days consecutively, and the median was chosen as an end result.

Table 1: Variation of XRD peak intensities, 2 theta, inter-planner distances (d) and planes for every sample with ultrasonic irradiation times.

Irradiation time (min)	Peak Intensity	2 Theta (degree)	d (hkl) (Å)	Plane (hkl)
0	3043	21.414	4.14616	110
	839	23.691	3.75255	200
5	2690	21.387	4.15131	110
	860	23.673	3.75541	200
10	1319	21.255	4.17688	110
	621	23.555	3.77396	200
15	2038	21.365	4.15555	110
	702	23.656	3.75802	200

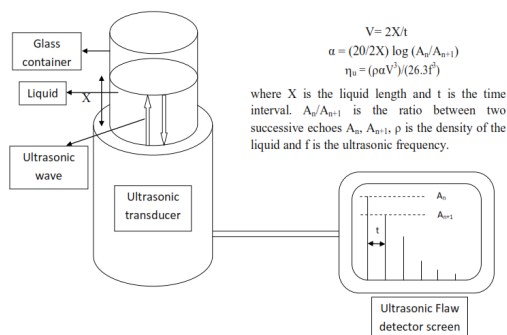


Fig. 1: Plot diagram for the ultrasonic pulse echo technique for measurement of ultrasonic velocity and ultrasonic absorption coefficient.

3. Results and discussions

The X-ray diffraction patterns for all LDPE samples at different ultrasound irradiation times, were recorded and shown in Fig. 2 and Table 1. The XRD patterns showed the characteristic peaks corresponding to orthorhombic crystalline planes (110) and (200) [12]. It can be seen from this figure, that the intensity of the peaks decreases with increasing irradiation time from 0 to 10 min and then increased at irradiation time 15 min.

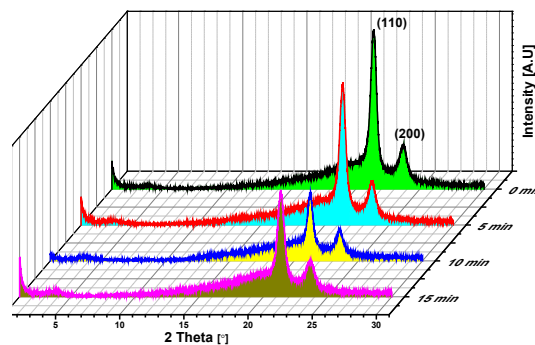


Fig. 2: X-ray diffraction patterns for LDPE samples at different irradiation times.

The variation of the calculated lattice parameters (a) and (b) were shown in Fig. 3 and Table 2. They increased with increasing the irradiation time up to 10 min, which means the increase in the inter-molecular distances, while they decreased at 15 min.

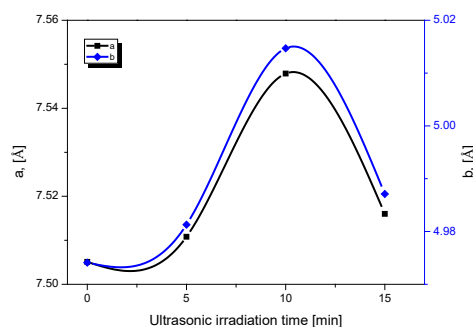


Fig. 3: Variation of lattice constants (a & b) for LDPE samples at different irradiation times.

Fig. 4 showed also the variation of crystallite size and the inter-chain distance, they showed the same behaviours as those of the lattice constants confirming the effect of the ultrasound irradiation in the formation of nano-LDPE (see Table 2). Mourad et al. [12] had reported that the increase in crystallite size is due to the further crystallization of small crystals and vice versa.

Table 2: Representation of crystallinity degree (%), lattice constants (a&b), full width at half maximum (FWHM), crystallite size (L) and inter-chain distance (D) with ultrasonic irradiation times.

Irradiation time (min)	Crystallinity degree (%)	a (Å)	B (Å)	FWHM	L (Å)	D (Å)
0	37.9	7.5051	4.9741	0.552	146.4	5.1853
5	36.4	7.5108	4.9813	0.537	150.5	5.1918
10	30.6	7.5479	5.0147	0.477	155.9	5.2236
15	35.7	7.5160	4.9871	0.590	137.0	5.1970

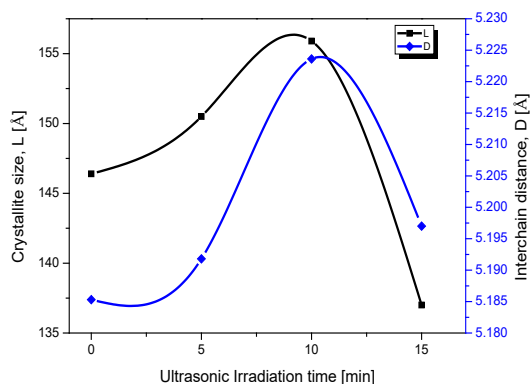


Fig. 4: Variation of the crystallite size and inter-chain distance for LDPE samples at different irradiation times.

Generally, the ultrasonic wave velocity depends on distance between atoms or molecules [21 & 24]. Therefore, the decrease in both (longitudinal and shear) ultrasonic wave velocities with the increase in ultrasonic irradiation time from 0 to 10 min as shown in Fig. 5 and Table 3, confirms the increase in inter-chain distances D and free length L_f (i.e. the increase in the distances between molecular surfaces). While the increased velocities at 15 minutes irradiation, interpret the decreased inter-chain distances. The change in ultrasonic velocity behaviours represents the good interaction throughout the entire composition range due to the chemical reactions between the constituents [21-24].

Table 3: Representation of density, both ultrasonic wave velocities (longitudinal and shear), ultrasonic absorption coefficient (α), ultrasonic viscosity, Poisson's ratio (σ), cross-link density (N_c) and free length (L_f) with ultrasonic irradiation times.

Irradiation time (min)	Density (kg/m ³)	U_l (m/s)	U_s (m/s)	α (dB/cm)	Viscosity (Pa.s)	σ	N_c	L_f (Å)
0	704	1603	816	1.61	41.2	0.325	0.550	8.243
5	809	1473	739	1.56	34.2	0.332	0.507	8.484
10	885	1298	626	1.24	18.1	0.348	0.417	9.557
15	817	1465	739	1.50	33.1	0.329	0.522	8.445

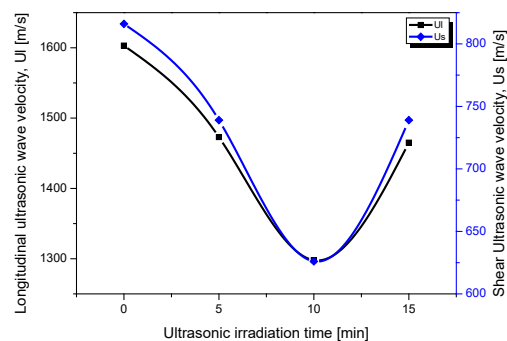


Fig. 5: Variation of both (longitudinal and shear) ultrasonic velocities for LDPE samples at different irradiation times.

Moreover, Fig. 6 showed the variation of both ultrasonic absorption coefficient and ultrasonic viscosity for all nano-LDPE samples. They decreased with increasing the irradiation time from 0 to 10 min, correlating with the decrease in ultrasonic wave velocities. At 15 min irradiation time, they increased due to the decrease in inter-chain distances (see Table 3). Huayue Wu et al. [25] had synthesized a nano-sized flake carboxymethyl cassava starch (CMCS) with high degree substitution under ultrasonic irradiation. The substitution degree of carboxymethylation and sonication time had a great influence on the morphology and the size of CMCS. Xiong Liang et al. [26] had plasticized the ultra-high molecular weight polyethylene (UHMWPE) semi-crystalline polymer using ultrasonic irradiation. They reported that the (UHMWPE) consists of nascent and melt-recrystallized phases and that energy concentrated at particle interfaces as a result of high-frequency friction, compressive deformation, and ultrasonic radiation led to rapid diffusion and interpenetration of the chain segment. Shaohua Chen et al. [27] had

investigated the influence of ultrasonic irradiation on the conformation and crystallization behaviors of two isotactic polypropylene samples with similar molecular weight and average isotacticity, but different stereo-defect distributions. The ultrasonic treatment induced a decrease in the degree of crystalline perfection and a wider distribution range of the crystalline perfection of polypropylene.

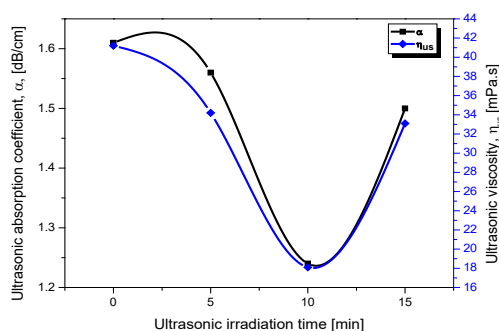


Fig. 6: Plot of the ultrasonic absorption coefficient and ultrasonic viscosity for LDPE samples at different irradiation times.

According to Rao [28], Poisson's ratio (σ) depends on the dimensionality of the structure and cross-link density. The cross-link density (N_c) was calculated according to Higazy & Bridge [29] using the following the equation:

$$\sigma = 0.28(N_c) - 0.25 \quad (4)$$

Therefore the decrease in Poisson's ratio as shown in Fig. 7 caused the decrease in cross-link density with the increase in ultrasonic irradiation time from 0 to 10 min. Further, the increase in cross-link density at 15 min confirms the polymer degradation at this time of irradiation.

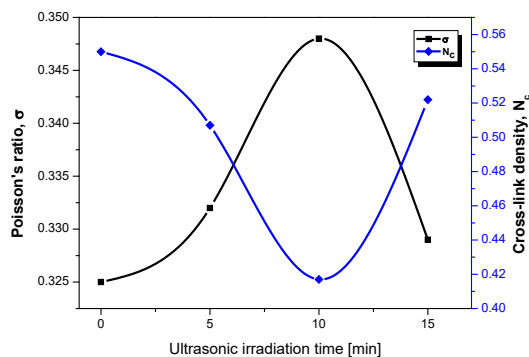


Fig. 7: Dependence of Poisson's ratio and cross-link density for LDPE samples at different irradiation times.

This behavior proved by ultrasonic measurement via decreasing in free length L_f (the distances between molecular surfaces).

Such results confirm indicate the formation of nano-LDPE using high power ultrasound at different times as polymerization initiator.

4. Conclusion

This research study showed the effect of the high power ultrasound to initiate the polymerization of LDPE in the nano-size. The results predicted the effect of ultrasound on the structure of these polymer samples. Also, the results of XRD and ultrasonic wave velocities were found to be in good agreement with each other.

Acknowledgement

The authors would like to express their sincere thanks to Majmaa University for supporting this search project. Also, they would like to express their thanks to the deanship of scientific research at the university.

References:

- [1]. I.G. Mikhailov, J. Struct. Chem, 9, 332, (1968)
- [2]. Donald L.Lamberson, Can.J. cham, 49, 611, (1971)
- [3]. N.G. Gereeze, Trans. Faraday Soc, 62, 112, (1966)
- [4]. Joongmin Shin, Xiaojing Liu, Naveen Chikthimma, Youn Suk Lee, Appl. Surface Sci., 386, 276, (2016).
- [5]. Trotignon. JP, Piperaud. M, Verdu. J, Dobraczynski. A, Summary of plastics, 5th ed, AFNOR 1991, p: 27-42.
- [6]. ISO-1872-1. Plastic – Polyéthylène (PE) moulding and extrusion materials. 1993 Part1: Désignation system and basis for spécifications.
- [7]. Nalwa HS. Handbook of low and high dielectric constant Materials and their applications-materials and processing, v.1. Academic, SanDiego. 1999
- [8]. Bartnikas R, Eichhorn RM. Engineering dielectrics. v.II A. ASTM Publications. Philadelphia. 1983
- [9]. Munaro M, L. Akcelrud L. Correlations between composition and crystallinity of LDPE/HDPE blends, J.Polym Res 2008 15:83–88.
- [10]. Füzessery S. Polyéthylène basse densité. No. A 3310. 1996. P. 7.
- [11]. Verdu. J, physical aging of plastics, 1990; A 3150 1-17.

- [12]. Mourad Hamouya, Aicha Mahir, Mohamed Chafik EL Idrissi, International Journal of Research in Engineering and Technology, 3 (2014) 210-215.
- [13]. G. V. Ramana Reddy, C. Ramesh Kumar, R. Sriram J Appl Polym Sci., 94, 739 (2004).
- [14]. F.D. Karia, P.H. Parsania, Eur. Polym. J, 36 (3), 519, (2000).
- [15]. R.K. Chowdoji, N.S.Venkata, R.A.Varada, Eur. Polym. J, 26(6), 657, (1990).
- [16]. R.A. Varada, R.K. Chowdoji and N. Venkata, Acoustica, 75, 213-216 (1991).
- [17]. L.E. Kinsler, A.R. Frey, A.B. Coppens, and J.V. Sanders, "Absorption and Attenuation of Sound, in: Fundamentals of Acoustics", 4th ed., pp. 210238, John Wiley & sons, New York, 2000.
- [18]. A.D. Pierce, "Basic Linear Acoustics, in: Springer Handbook of Acoustics", pp. 98-106, Springer 2007.
- [19]. B.O. Enflo, and C.M. Hedberg, "Physical Theory of Nonlinear Acoustics, in: Theory of Nonlinear Acoustics in Fluids, Fluid Mechanics and its Applications", vol. 67, pp. 11-30, Kluwer Academic Publishers 2004.
- [20]. C.M. Sehgal, J. Acoust. Soc. Am., 94, 1944, (1993).
- [21]. H.E.Nasr, M.S.Gaafar, O.Abdel-Kareem, F. Abd El-Aziz, J. American Science, 6(9), 897, (2010).
- [22]. M. A. Nour, M. S. Gaafar, A. Eid, A. A. El-Ebissy, 14TH EUROPEAN CONFERENCE ON COMPOSITE MATERIALS 7-10 June 2010, Budapest, Hungary.
- [23]. B. M. Teo, M. Ashok Kumar, F. Grieser, J. Phys. Chem. Lett., 112, 5265 (2008).
- [24]. Y. Mori, R. Saito, Polymer, 45, 95, (2004).
- [25]. Wenxia Gao, Xiaoqing Lin, Xiepeng Lin, Jinchang Ding, Xiaobo Huang, Huayue Wu, Carbohydrate Polymers, 84, 1413, (2011).
- [26]. Xiong Liang, Xiaoyu Wu, Kun Zeng, Bin Xu, Shiyun Wu, Hang Zhao, Bing Li, Shuangchen Ruan, J. of Micromechanics and Microengineering, 24, 045014, (2014).
- [27]. Shaohua Chen, Yuansen Liu, Tao Zeng, Nannan Duan, Zhi Wang, Luoxin Wang, Hua Wang, Changan Xu, Jian Kang, Polymer Science Series A, 57, 565, (2015).
- [28]. K. Rao, "Structural Chemistry of Glasses", (North Holland: Elsevier), (2002).
- [29]. A. A. Higazy, B. Bridge, J. Non-Cryst. Solids, (1985), 72, 81.

The Photogravitational Circular Restricted Four-body Problem with Variable Masses

Abdullah A. Ansari

Department of Mathematics , College of Science, Majmaah University, Al-Zulfi, Kingdom of Saudi Arabia,

a.ansari@mu.edu.sa

Abstract

In this paper, we examine the stability of the equilibrium points in the photogravitational circular restricted four-body problem by considering all the masses are varying with time, one of the three masses are taken as source of radiation pressure and all the masses are placed at the vertices of an equilateral triangle. We derive the equations of motion under the effect of solar radiation pressure by using the Meshcherskii transformations. We have plotted the equilibrium points, time series, surfaces of motion of infinitesimal body, Poincare surface of sections and Newton-Raphson basin of attraction. Here five equilibrium points are found but it is ten in the classical case. From the time series, it is observed that the orbit will not be periodic. The surfaces of motion of the infinitesimal body are studied in the space. The Poincare surface of section is in the discrete type of pattern. The convergence of the equilibrium points is studied by the Newton-Raphson basin of attraction. Finally, we have examined the stability of the equilibrium points and found that all the equilibrium points are unstable.

Keywords: Radiation Pressure; variable masses; equilateral triangle; Poincare surface of sections; Newton-Raphson basin of attraction.

1. Introduction

The restricted problem is studied by many scientists and mathematicians in the two-body, three-body, four-body and N-body models. Chernikov [8] investigated the stability of equilibrium points by Lyapunov's methods in the restricted three body problem (Sun-Planet-Particle) with the effects of solar radiation pressure. Perezhogin [17] studied the stability of the sixth and seventh libration points in the photogravitational circular restricted three body problem. Bhatnagar et al. [7] studied about the lagrangian points in the photogravitational restricted three body problem. They examined the stability of the equilibrium points and observed that the equilibrium points are stable in the linear sense and unstable around the triangular points. Mignard [14] studied the restricted three-body problem with the inclusion of solar radiation pressure. And observed that triangular equilibrium points are no longer exist. Simmons [20] investigated the restricted 3-body problem with radiation pressure and observed that nine equilibrium points exists, five in the plane of motion and four in the out of plane. Sharma [19] investigated the variation of the solar radiation pressure and oblateness factor on the stationary solutions of the planar restricted three-body problem when the more massive primary is a source of radiation and smaller primary is an oblate spheroid with its equatorial plane coincident with the plane of motion. AbdulRaheem et al. [4] investigated the stability of equilibrium points under the influence of the Coriolis and centrifugal forces together with the effects of oblateness and radiation pressure of the primaries. It is observed that the collinear points are unstable and the triangular points are conditionally stable

depending on the radiation factor and oblateness. It is also observed that the Coriolis force has a stabilizing tendency, while the centrifugal force, radiation and oblateness of the primaries have destabilizing effects. Kalvouridis, et al. [10] investigated the dynamical properties and the parametric evolution of periodic orbits in the restricted four body problem with radiation pressure. They illustrated the zero-velocity curves and surfaces and also they examined the stability of the equilibrium points. Abouelmagd [2] investigated the stability and periodic orbits in the restricted three body problem under the effects of oblateness and radiation pressure. He observed that the collinear points are unstable while triangular points are conditionally stable depending on the radiation pressure and oblateness. And also the elements of periodic orbits around equilibrium points are affected by oblateness. Singh, et al. [25] studied numerically the restricted four-body problem by considering all the primaries as source of radiation pressure, placed at the vertices of an equilateral triangle. They observed that the equilibrium points are unstable. Pushparaj, et al. [18] studied the interior resonance periodic orbits around the Sun in the photogravitational restricted three body problem by the method of Poincare surface of section. They observed that the period of time decrease with the increase of radiation pressure.

Many researchers have explored about the variable masses and the Newton-Raphson basins of attraction as Meshcherskii [13], Lichtenegger[12] Singh [21, 22, 23, 24], Douskos [9], Zhang [26], Kumari [11], Assis [5], Abouelmagd [3], Mittal [15], Zotos [27, 28, 29, 30].

We have studied the circular restricted four-body problem in which the masses of the primaries as well as the mass of the infinitesimal body vary with time and one of the primaries is taken as source of radiation pressure. We have discussed our problem in various sections. In the first section, we have reviewed the literature. In the second section, we have derived the equations of motion of the infinitesimal variable mass under the effects of the radiation pressure. In the third section, we have illustrated the numerical analysis (equilibrium points, time series, surface of motion of the infinitesimal body, Poincare surface of section and Newton-Raphson basin of attraction). In the fourth section, we have examined the stability of the equilibrium points. Finally, in the fifth section, we have concluded the problem. Our problem has great applications in the Astronomy and Astrophysics.

2. Equations of motion

Let m_1, m_2 and m_3 be the masses of the three primaries, placed at the vertices of an equilateral triangle of side ℓ . The fourth infinitesimal body having mass m , moving under the influence of the primaries but not influencing them. The one of the primaries as m_2 is considered as source of radiation pressure with factor q and all the masses are varying with time. The primaries are revolving in the circular orbits around their center of mass which is considered as origin. The primary m_1 is placed at x -axis, the line passing through the origin and perpendicular to the x -axis, is taken as y -axis and the line passing through the origin and perpendicular to the plane of motion of the primaries is taken as z -axis (Fig. 1). Initially, we supposed that the synodic plane coincides with the inertial plane and revolving with mean motion ω about z -axis. Using the procedure of Abdullah [1], we can write the equations of motion of the variable infinitesimal body in the restricted four body problem as

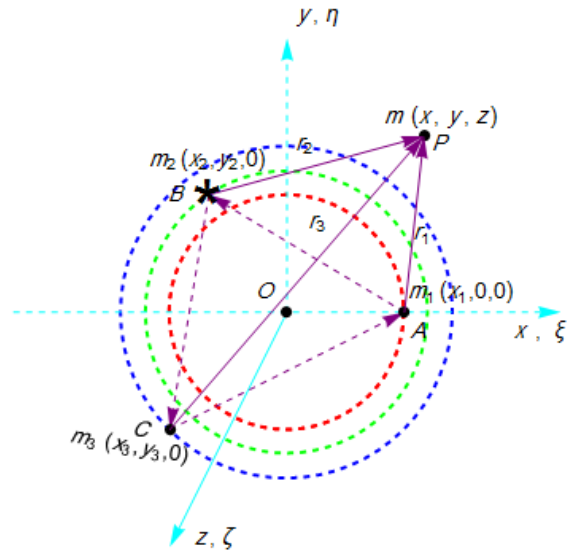


Fig. 1: Configuration of the circular restricted four-body problem with solar radiation pressure at B.

$$\frac{\dot{m}}{m}(\ddot{x} - \omega^2 x) + (\ddot{y} - \dot{\omega} y - 2\omega \dot{x} - \omega^2 y) = -\frac{m_1 G(x - x_1)}{r_1^3} - \frac{m_2 G(x - x_2)q}{r_2^3} - \frac{m_3 G(x - x_3)}{r_3^3},$$

$$\frac{\dot{m}}{m}(\dot{y} + \omega x) + (\ddot{y} + \dot{\omega} x + 2\omega \dot{x} - \omega^2 y) = -\frac{m_1 G(y - y_1)}{r_1^3} - \frac{m_2 G(y - y_2)q}{r_2^3} - \frac{m_3 G(y - y_3)}{r_3^3},$$

$$\frac{\dot{m}}{m}\ddot{z} + \ddot{z} = -\frac{m_1 Gz}{r_1^3} - \frac{m_2 Gzq}{r_2^3} - \frac{m_3 Gz}{r_3^3},$$

where,

$$r_i^2 = (x - x_i)^2 + (y - y_i)^2 + z^2, (i = 1, 2, 3),$$

are the distances from the primaries to the infinitesimal body, G is the gravitational constant.

Let $\mu_i(t) = m_i G, (i = 1, 2, 3)$.

Using Meshcherskii transformation [13],

$$x = \xi R(t), y = \eta R(t), z = \zeta R(t),$$

$$\frac{dt}{d\tau} = R^2(t), r_i = \rho_i R(t),$$

$$\omega(t) = \frac{\omega_0}{R^2(t)}, x_i = \xi_i R(t), y_i = \eta_i R(t),$$

$$\mu(t) = \frac{\mu_0}{R(t)}, \mu_i(t) = \frac{\mu_{i0}}{R(t)},$$

$$m = \frac{m_0}{R(t)}, R(t) = \sqrt{at^2 + 2bt + c},$$

$$ac - b^2 = 1 - k, \quad (i = 1, 2, 3),$$

where $k, a, b, c, \mu_0, \mu_{10}, \mu_{20}, \mu_{30}, m_0$ are constants.

Considering unit of mass, distance and time at initial time t_0 such that

$$\mu_0 = 1, \ell = 1, \omega_0 = 1, G = 1, a t_0 + b = \alpha_1 \text{ (constant)}$$

Introducing the mass parameter as

$$\mu_{10} = \mu, \mu_{20} = (1 - \mu - \alpha_2 \mu), \mu_{30} = \alpha_2 \mu, \alpha_2 \ll 1,$$

Finally, the equations of motion become

$$\xi'' - 2\eta' - \alpha_1 \xi' = \Omega_\xi,$$

$$\eta'' + 2\xi' - \alpha_1 \eta' = \Omega_\eta,$$

$$\zeta'' - \alpha_1 \zeta' = \Omega_\zeta. \quad (1)$$

where,

$$\Omega = \frac{1}{2}(\alpha_1^2 + k)(\xi^2 + \eta^2 + \zeta^2) - \frac{1}{2}\zeta^2$$

$$- \alpha_1 \xi \eta + \frac{\mu}{\rho_i^2} + \frac{(1 - \mu - \alpha_2 \mu)q}{(\xi - \xi_i)^2 + (\eta - \eta_i)^2 + \zeta^2} + \frac{\alpha_2 \mu}{\rho_3},$$

$$(\xi_1, \eta_1) = \left(\frac{1}{\sqrt{3}}, 0\right), (\xi_2, \eta_2) = \left(-\frac{1}{2\sqrt{3}}, \frac{1}{2}\right),$$

$$(\xi_3, \eta_3) = \left(-\frac{1}{2\sqrt{3}}, -\frac{1}{2}\right).$$

Prime (') is the differentiation w.r.t. τ .

3. Numerical Analysis

3.1 Equilibrium points

The equilibrium points can found by taking

$$\xi'' = \xi' = \eta'' = \eta' = \zeta'' = \zeta' = 0 \text{ in equation (1),}$$

i.e.

$$(\alpha_1^2 + k)\xi - \alpha_1 \eta - \frac{\mu(\xi - \xi_1)}{\rho_1^3}$$

$$- \frac{(1 - \mu - \alpha_2 \mu)(\xi - \xi_2)q}{\rho_2^3} - \frac{\alpha_2 \mu(\xi - \xi_3)}{\rho_3^3} = 0, \quad (2)$$

$$(\alpha_1^2 + k)\eta - \alpha_1 \xi - \frac{\mu \eta}{\rho_1^3}$$

$$- \frac{(1 - \mu - \alpha_2 \mu)(\eta - \eta_2)q}{\rho_2^3} - \frac{\alpha_2 \mu(\eta - \eta_3)}{\rho_3^3} = 0, \quad (3)$$

$$(\alpha_1^2 + k - 1)\zeta - \frac{\mu \zeta}{\rho_1^3} - \frac{(1 - \mu - \alpha_2 \mu)\zeta q}{\rho_2^3}$$

$$- \frac{\alpha_2 \mu \zeta}{\rho_3^3} = 0. \quad (4)$$

We have shown the equilibrium points graphically in (ξ, η) plane (Fig. 2), (ξ, ζ) plane (Fig. 3) and (η, ζ) plane (Fig. 4). In the (ξ, η) plane, we found five equilibrium points. The green dots denote the locations of the equilibrium points and the purple dots denote the locations of the primaries. But Baltagiannis [6] have gotten ten equilibrium points with unequal masses in the classical case. In the (ξ, ζ) plane, we found five equilibrium points. The green dots denote the locations of the equilibrium points. In the (η, ζ) plane, we found three equilibrium points. The black dots denote the locations of the equilibrium points.

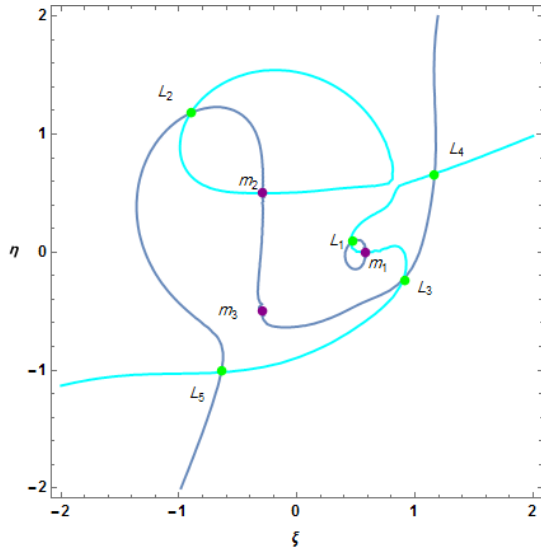


Fig. 2: Locations of equilibrium points at
 $\alpha_1 = 0.2, k = 0.4, \alpha_2 = 0.01, \mu = 0.019, q = 0.8.$

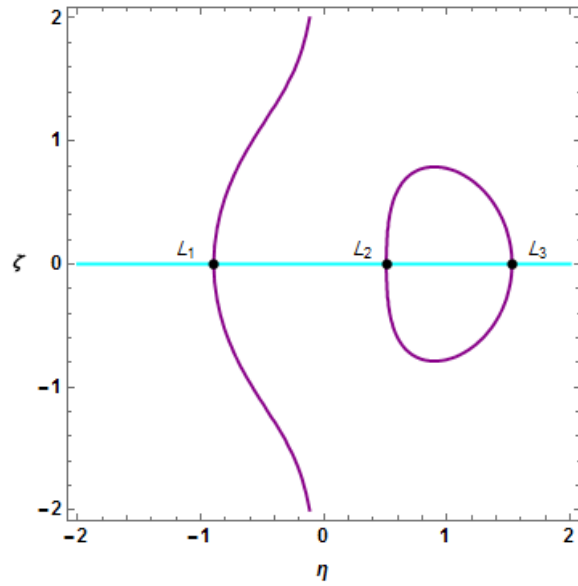


Fig. 4: Locations of equilibrium points at
 $\alpha_1 = 0.2, k = 0.4, \alpha_2 = 0.01, \mu = 0.019, q = 0.8.$

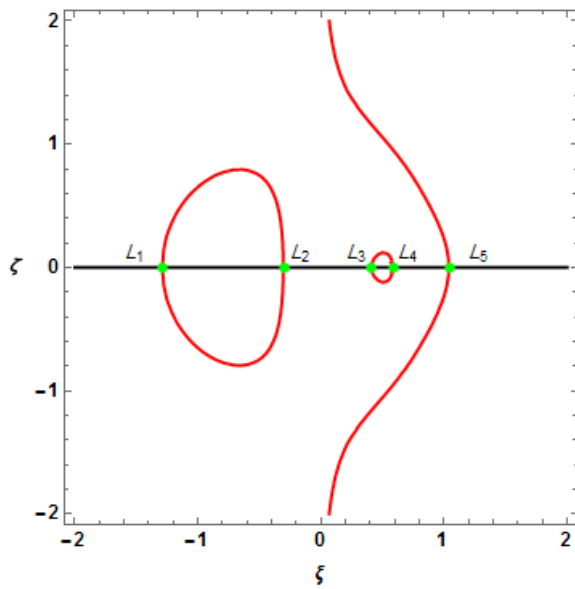


Fig. 3: Locations of equilibrium points at
 $\alpha_1 = 0.2, k = 0.4, \alpha_2 = 0.01, \mu = 0.019, q = 0.8.$

3.2 Time series

We have plotted the time series in between (τ, ξ) (Fig. 5.) and (τ, η) (Fig. 6). These time series show that the orbits will not be periodic.

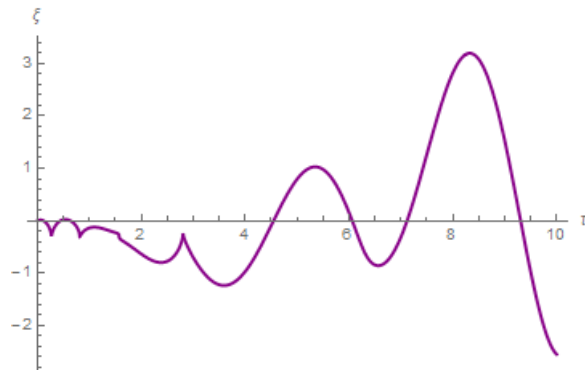


Fig. 5: Time series in between (τ, ξ) at
 $\alpha_1 = 0.2, k = 0.4, \alpha_2 = 0.01, \mu = 0.019, q = 0.8.$

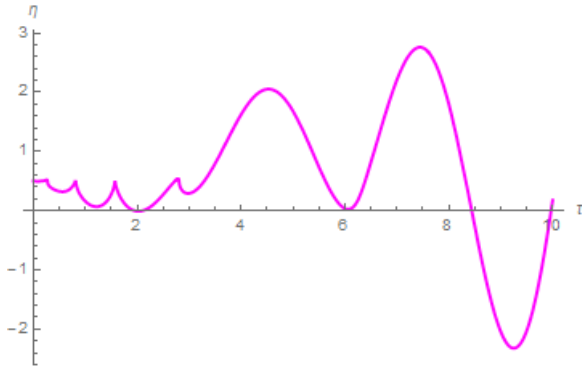


Fig. 6. Time series in between (τ, η) at

$\alpha_1 = 0.2, k = 0.4, \alpha_2 = 0.01, \mu = 0.019, q = 0.8.$

3.3 Surfaces

i. Surfaces of the motion of the infinitesimal body

In this section, we have drawn the surface of motion of the infinitesimal body by considering the equations (2 and 3) (Fig. 7), the equations (2 and 4) (Fig. 8), the equations (3 and 4) (Fig. 9).

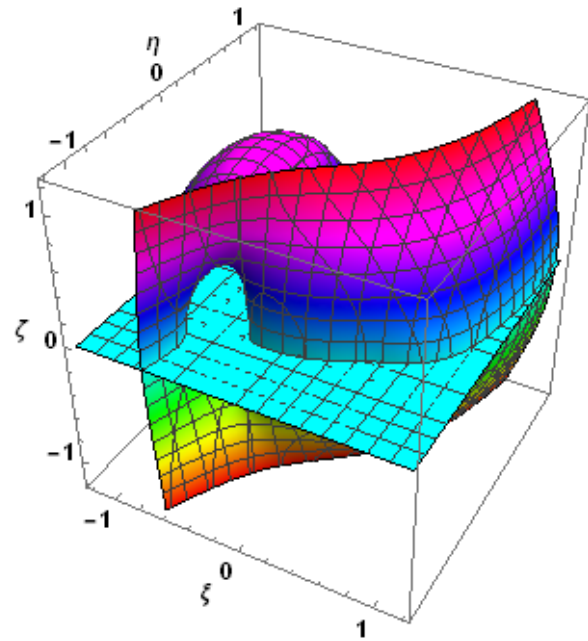


Fig. 8. The surface of motion of the infinitesimal body in $(\xi, \eta = 0, \zeta)$ -plane

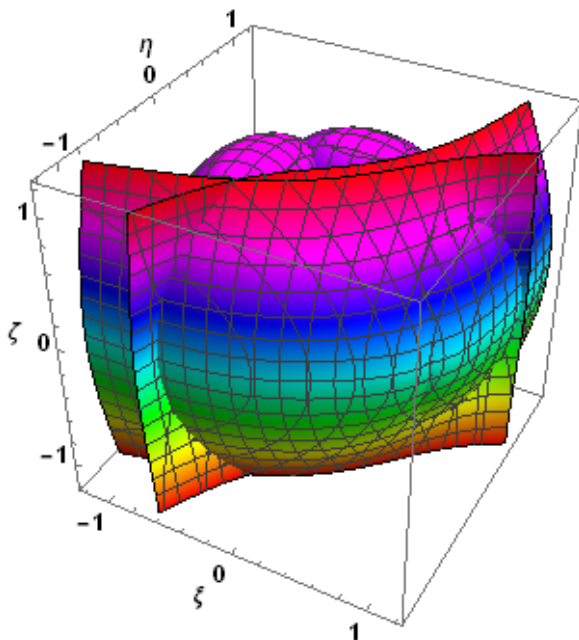


Fig. 7. The surface of motion of the infinitesimal body in $(\xi, \eta, \zeta = 0)$ -plane

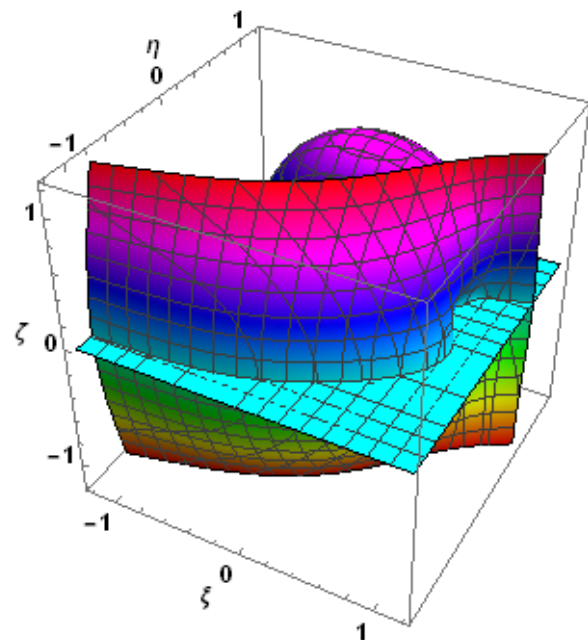


Fig. 9. The surface of motion of the infinitesimal body in $(\xi = 0, \eta, \zeta)$ -plane

ii. Poincare surface of section

We have drawn the Poincare surface of section and got a discrete type of graph (Fig. 10).

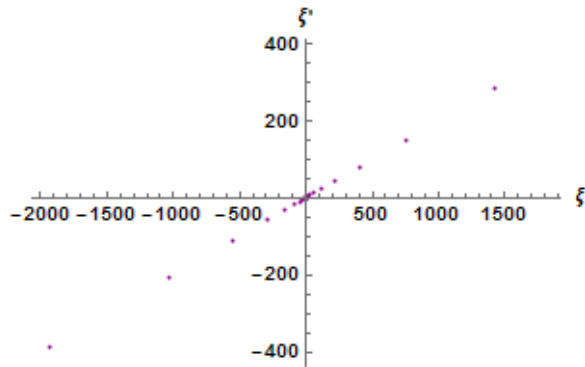


Fig. 10: Poincare surface of section

3.4 Newton-Raphson basin of attraction

We have drawn the basins of attraction by using the simple and accurate Newton-Raphson iterative method for solving systems of equation. This method is also applicable for systems of multivariate functions. The iterative algorithm of our problem is given by the system

$$\begin{aligned} \xi_n &= \xi_{n-1} - \left(\frac{\Omega_{\xi\xi} \Omega_{\eta\eta} - \Omega_{\eta\xi} \Omega_{\xi\eta}}{\Omega_{\xi\xi} \Omega_{\eta\eta} - \Omega_{\xi\eta} \Omega_{\eta\xi}} \right)_{(\xi_{n-1}, \eta_{n-1})}, \\ \eta_n &= \eta_{n-1} - \left(\frac{\Omega_{\eta\xi} \Omega_{\xi\xi} - \Omega_{\xi\xi} \Omega_{\eta\xi}}{\Omega_{\xi\xi} \Omega_{\eta\eta} - \Omega_{\xi\eta} \Omega_{\eta\xi}} \right)_{(\xi_{n-1}, \eta_{n-1})}. \end{aligned} \quad (5)$$

Where ξ_{n-1}, η_{n-1} are the values of the ξ and η coordinates of the $(n-1)$ _{th} step of the Newton-Raphson iterative process. The initial point (ξ, η) is a member of the basin of attraction of the root if this point converges rapidly to one of the equilibrium points. This process stops when the successive approximation converges to an attractor, with some predefined accuracy. For the classification of the equilibrium points on the (ξ, η) plane, we will use color code. In this way a complete view of the basin structures created by the attractors (Fig. 11). Also we have shown the zoomed part of the basins of attractions near the primaries (Fig. 12). We used Mathematica software for finding basin of attraction.

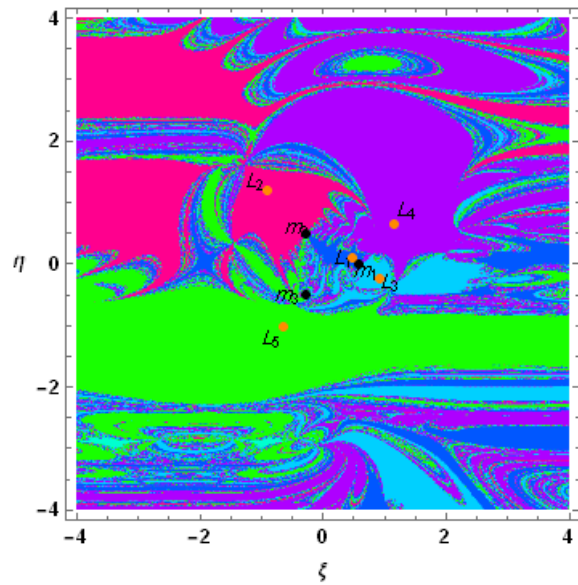


Fig. 11: Newton-Raphson basin of attraction under the effects of solar radiation pressure where orange dots indicate the locations of the equilibrium points and black dots indicate the locations of the primaries.

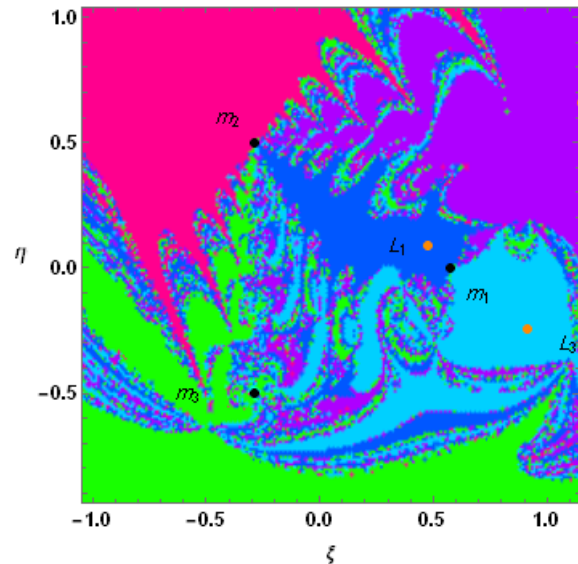


Fig. 12: The zoomed part of Fig. 11 near the primaries.

4. Stability

Using the procedure given by Mccuskey [16], we can examine the stability of the equilibrium points in the photogravitational circular restricted four-body problem. Let us suppose

$\xi = \xi_0 + \alpha, \eta = \eta_0 + \beta, \zeta = \zeta_0 + \gamma$, putting these values in equation (1), we get

$$\begin{aligned} \alpha'' - 2\beta' - \alpha_1\alpha' &= \alpha \Omega_{\xi\xi}^0 + \beta \Omega_{\xi\eta}^0 + \gamma \Omega_{\xi\zeta}^0, \\ \beta'' + 2\alpha' - \alpha_1\beta' &= \alpha \Omega_{\eta\xi}^0 + \beta \Omega_{\eta\eta}^0 + \gamma \Omega_{\eta\zeta}^0, \\ \gamma'' - \alpha_1\gamma' &= \alpha \Omega_{\zeta\xi}^0 + \beta \Omega_{\zeta\eta}^0 + \gamma \Omega_{\zeta\zeta}^0, \end{aligned} \quad (6)$$

Where α, β and γ are the small displacements of the infinitesimal body from the equilibrium points. Suffix zero denotes the value at the equilibrium point.

To solve equation (6), let

$$\alpha = Ae^{\lambda\tau}, \beta = Be^{\lambda\tau}, \gamma = Ce^{\lambda\tau},$$

where A, B and C are parameters.

After substituting these values in equation (6), we get

$$\begin{aligned} A(\lambda^2 - \alpha_1\lambda - \Omega_{\xi\xi}^0) - B(2\lambda + \Omega_{\xi\eta}^0) - C\Omega_{\xi\zeta}^0 &= 0, \\ A(2\lambda - \Omega_{\eta\xi}^0) + B(\lambda^2 - \alpha_1\lambda - \Omega_{\eta\eta}^0) - C\Omega_{\eta\zeta}^0 &= 0, \\ -A\Omega_{\zeta\xi}^0 - B\Omega_{\zeta\eta}^0 + C(\lambda^2 - \alpha_1\lambda - \Omega_{\zeta\zeta}^0) &= 0, \end{aligned} \quad (7)$$

The equation (7) will have a non-trivial solution for A, B and C, if

$$\begin{vmatrix} \lambda^2 - \alpha_1\lambda - \Omega_{\xi\xi}^0 & -(2\lambda + \Omega_{\xi\eta}^0) & -\Omega_{\xi\zeta}^0 \\ 2\lambda + \Omega_{\eta\xi}^0 & \lambda^2 - \alpha_1\lambda - \Omega_{\eta\eta}^0 & -\Omega_{\eta\zeta}^0 \\ -\Omega_{\zeta\xi}^0 & -\Omega_{\zeta\eta}^0 & \lambda^2 - \alpha_1\lambda - \Omega_{\zeta\zeta}^0 \end{vmatrix} = 0,$$

$$\begin{aligned} \lambda^6 - 3\alpha_1\lambda^5 + \lambda^4(4 + 3\alpha_1^2 - \Omega_{\xi\xi}^0 - \Omega_{\eta\eta}^0 - \Omega_{\zeta\zeta}^0) \\ + \lambda^3(-4\alpha_1 - \alpha_1^3 + 2\alpha_1\Omega_{\xi\xi}^0 + 2\alpha_1\Omega_{\eta\eta}^0 + 2\alpha_1\Omega_{\zeta\zeta}^0 \\ + 4\Omega_{\xi\eta}^0) + \lambda^2((\Omega_{\xi\eta}^0)^2 - (\Omega_{\xi\zeta}^0)^2 + \Omega_{\xi\xi}^0\Omega_{\eta\eta}^0 \\ - (\Omega_{\eta\zeta}^0)^2 - 4\Omega_{\zeta\xi}^0 + \Omega_{\xi\xi}^0\Omega_{\zeta\zeta}^0 + \Omega_{\zeta\zeta}^0\Omega_{\eta\eta}^0 \\ + 4\alpha_1\Omega_{\xi\eta}^0 - \alpha_1^2(\Omega_{\xi\xi}^0 + \Omega_{\eta\eta}^0 + \Omega_{\zeta\zeta}^0)) \\ + \lambda(-4\Omega_{\xi\eta}^0\Omega_{\zeta\zeta}^0 - \alpha_1(\Omega_{\xi\eta}^0)^2 + \alpha_1(\Omega_{\xi\zeta}^0)^2 \\ - \alpha_1\Omega_{\xi\xi}^0\Omega_{\eta\eta}^0 + \alpha_1(\Omega_{\eta\zeta}^0)^2 - \alpha_1\Omega_{\xi\xi}^0\Omega_{\zeta\zeta}^0 \\ - \alpha_1\Omega_{\eta\eta}^0\Omega_{\zeta\zeta}^0) + ((\Omega_{\xi\zeta}^0)^2\Omega_{\eta\eta}^0 + \Omega_{\xi\xi}^0(\Omega_{\eta\zeta}^0)^2 \\ - (\Omega_{\xi\eta}^0)^2\Omega_{\zeta\zeta}^0 - \Omega_{\xi\xi}^0\Omega_{\eta\eta}^0\Omega_{\zeta\zeta}^0) = 0, \end{aligned} \quad (8)$$

Table 1: Eigen Values

Coordinate of Equilibrium Points (ξ, η)	Eigen Values (λ)
L_1 (0.34846, 0.09071)	{-1.3645491647931514 - 2.1750266263845335i}, {-1.3645491647931514 + 2.1750266263845335i}, {0.1 - 1.9052998624502675i}, {0.1 + 1.9052998624502675i}, {0.915627074598914}, {2.2134712549873887}}
L_2 (-1.07658, 1.3532)	{-0.4049887442604912 - 1.7442855728866289i}, {-0.4049887442604912 + 1.7442855728866289i}, {0.1 - 1.0261111757589274i}, {0.1 + 1.0261111757589274i}, {0.6049887442604907 - 0.2541475139791303i}, {0.6049887442604907 + 0.2541475139791303i}, {-0.17593511143553683 - 1.6967217827520438i}, {-0.17593511143553683 + 1.6967217827520438i},
L_3 (1.07658, -0.30168) (1.07658, -0.30168)	{0.1 - 0.9185358306204258i}, {0.1 + 0.9185358306204258i}, {0.3759351114355368 - 0.28232515163735344i}, {0.3759351114355368 + 0.28232515163735344i}
L_4 (1.36342, 0.873978)	{0.012372274711160473 - 0.2854727328040165i}, {0.012372274711160473 + 0.2854727328040165i}, {0.1 - 0.8503875379646464i}, {0.1 + 0.8503875379646464i}, {0.18762772528883953 - 1.6913614606518697i}, {0.18762772528883953 + 1.6913614606518697i}
L_5 (-0.8368, -1.1946)	{0.009779043058938596 - 0.2850394466860824i}, {0.009779043058938596 + 0.2850394466860824i}, {0.1 - 0.831952106427792i}, {0.1 + 0.831952106427792i}, {0.19022095694106142 - 1.700849155153382i}, {0.19022095694106142 + 1.700849155153382i}

We solved the equation (8) for all the values of the equilibrium points and for each equilibrium point, we found six eigenvalues in which at least one is either positive real value or positive real part of the eigenvalues (Table 1). Therefore, all the equilibrium points are unstable.

5. Conclusions

In this paper, we explore the locations and stability of the circular restricted four-body problem by supposing all the masses are varying with time and one of the masses is source of radiation pressure. The three primaries are placed at the vertices of an equilateral triangle and revolving around their center of mass which is taken as origin. We derive the equations of

motion which are different from the classical case by the factors α_1 and k . We have plotted the graphs for the locations of the equilibrium points in three planes, the time series, the surfaces and the Newton-Raphson basin of attraction. In the (ξ, η) plane, we found five equilibrium points (Fig. 2) which are ten in the classical case, where the green dots denote the locations of the equilibrium points and the purple dots denote the locations of the primaries. In the (ξ, ζ) plane, we found five equilibrium points (Fig. 3) where the green dots denote the locations of the equilibrium points. In the (η, ζ) plane, we found three equilibrium points (Fig. 4) where the black dots denote the locations of the equilibrium points. From the time series, we observed that the orbits are not periodic (Fig. 5 & 6). We have drawn the surfaces of the motion of the infinitesimal body in three spaces (Figs. 7, 8, 9) and the Poincare surface of section where we got discrete type graph (Fig. 10). We also have drawn the Newton-Raphson basin of attraction (Fig. 11), where we have shown the convergence of the equilibrium points and the locations of equilibrium points are indicated by orange dots and the locations of the primaries are indicated by black dots. The Fig. 12 is the zoomed part of the Fig. 11 near the primaries. Zotos [27, 28, 29, 30] are illustrated basins of attraction in the classical case and they found scorpion type graph which is different from my case. Finally, we examine the stability of the equilibrium points for the circular restricted four-body problem with radiation pressure and found at least one positive real value or one positive real part of the eigenvalues (Table 1). Hence all the equilibrium points are unstable.

Acknowledgements

We are thankful to the Deanship of scientific research and the department of Mathematics, College of Science, Al-Zulfi, Majmaah University, Kingdom of Saudi Arabia for providing all the facilities in the completion of this research work.

References

- [1]. Abdullah, (2017). Dynamics in the circular restricted three body problem with perturbations. International Journal of Advanced Astronomy. vol. 5, no. 1, pp. 19-25.
- [2]. Abouelmagd, E. I., Sharaf, M.A., (2013). The motion around the libration points in the restricted three-body problem with the effect of radiation and oblateness. Astrophys. Space sci. vol. 344, pp. 321-332.
- [3]. Abouelmagd, E. I., Mostafa, A., (2015). Out of plane equilibrium points locations and the forbidden movement regions in the restricted three-body problem with variable mass. *Astrophysics Space Sci.* 357, 58. DOI 10.1007/s10509-015-2294-7.
- [4]. AbdulRaheem, A., Singh, J., (2006). Combined effects of perturbations, radiation and oblateness on the stability of equilibrium points in the restricted three-body problem. The Astronomical Journal. 131, 1880-1885.
- [5]. Assis, S. C., et al., (2014). Escape dynamics and fractal basin boundaries in the planar earth-moon system, *Celest. Mech. Dyn. Astr.*, 120, 105-130.
- [6]. Baltagiannis, A.N., Papadakis, K.E. (2011). Equilibrium points and their stability in the restricted four-body problem. *Int. J. Bifurc. Chaos* 21, 2179.
- [7]. Bhatnagar, K. B., Chawla, J. M., (1979). A study of the Lagrangian points in the photogravitational restricted three body problem. *Indian journal of pure and applied mathematics.* Vol. 10, pp. 1443-1451.
- [8]. Chernikov, Yu. A., (1970). The Photogravitational restricted three body problem, *Soviet Astronomy*, 14(1), pp. 176-181.
- [9]. Douskos, C. N., (2010). Collinear equilibrium points of Hill's problem with radiation pressure and oblateness and their fractal basins of attraction. *Astrophys. Space Sci.* 326, 263-271.
- [10]. Kalvouridis, T., Arribus, M., Elike, A., (2007). Parametric evolution of periodic orbits in the restricted four body problem with radiation pressure. *Planetary and space science.* Vol. 55, pp. 475-493.
- [11]. Kumari, R., Kushvah, B. S., (2014). Stability regions of equilibrium points in the restricted four body problem with oblateness effects. *Astrophysics Space Sci.*, 349, 693-704.
- [12]. Lichtenegger, H., (1984) The dynamics of bodies with variable masses. *Celest. Mech.* 34, 357-368.
- [13]. Meshcherskii, I.V., (1949). Studies on the Mechanics of Bodies of Variable Mass. *GITTL, Moscow*.
- [14]. Mignard, F., (1984) Stability of L_4 and L_5 against radiation pressure. *Celest. Mech.* 34, 275-287.
- [15]. Mittal, A., et. al., (2016) Stability of libration points in the restricted four-body problem with variable mass. *Astrophysics and space sci.* 361, 329. DOI 10.1007/s10509-016-2901-2.
- [16]. Mccuskey, S. W., (1963). Introduction to Celestial Mechanics. *Addison-Wesley, USA*.
- [17]. Perezhogin, A. A., (1976). Stability of the sixth and seventh libration points in the photogravitational restricted circular three body problem. *Soviet Astronomy letters.* Vol 2, pp. 172.
- [18]. Pushparaj, N., Sharma, R. K., (2017). Interior resonance periodic orbits in the photogravitational restricted three-body problem. *Advances in astrophysics.* Vol. 1(2), pp. 25-34.
- [19]. Sharma, R. K., (1987). The linear stability of libration points of the photogravitational restricted three body problem when the smaller primary is an oblate spheroid. *Astrophys. Space Sci.* vol.135, pp. 271-281.
- [20]. Simmons, J. F. L., McDonald, A. J. C., Brown, J. C., (1985). The restricted three body problem with radiation pressure. *Celestial Mechanics.* Vol. 35, pp. 145-187.
- [21]. Singh, J. et al. (1984). Effect of perturbations on the location of equilibrium points in the restricted problem of three bodies with variable mass. *Celest. Mech.* 32 (4), 297-305.
- [22]. Singh, J., Ishwar, B., (1985). Effect of perturbations on the

- stability of triangular points in the restricted problem of three bodies with variable mass. *Celest. Mech.* 35, 201-207.
- [23]. Singh, J., Leke, O., (2010). Stability of photogravitational restricted three body problem with variable mass. *Astrophysics and Space Sci.* 326 (2), 305-314.
- [24]. Singh, J., Leke, O., (2013). Existence and Stability of Equilibrium Points in the Robe's Restricted Three-Body Problem with Variable Masses. *International Journal of Astronomy and Astrophysics.* 3, 113-122.
<http://dx.doi.org/10.4236/ijaa.2013.32013>. [25]
- [26]. Singh J., Vincent, A. E., (2016) Equilibrium points in the restricted four-body problem with radiation pressure. *Few-Body Syst.* 57, 83-91.
- [27]. Zhang, M. J., Zhao, C. Y., Xiong, Y. Q., (2012). On the triangular libration points in photo-gravitational restricted three body problem with variable mass. *Astrophysics Space Sci.*, 337, 107-113. DOI 10.1007/s10509-011-0821-8.
- [28]. Zotos, E. E., (2016). Fractal basins of attraction in the planar circular restricted three body problem with oblateness and radiation pressure, *Astrophys. Space Sci.*, 181, 17.
- [29]. Zotos, E. E., (2016). Fractal basins boundaries and escape dynamics in a multi-well potential, *Non-linear Dyn.*, 85, 1613-1633.
- [30]. Zotos, E. E., (2016). Investigating the Newton-Raphson basins of attraction in the restricted three body problem with modified Newtonian gravity, *J. Appl. Math. Comput.*, Oct., 1-19.
- [31]. Zotos, E. E., (2017). Revealing the basins of convergence in the planar equilateral restricted four body problem, *Astrophys. Space Sci.*, 362, 2

Journal of Engineering and Applied Sciences (JEAS)

- **Space Air- Conditioning by Aqua Ammonia Absorption System using Exhaust Waste Heat of Diesel Generator Set**

Vakkar Ali and Ziaur Rehman

- **Synthesis, Characterization and Efficiency of Alum Produced from Waste Aluminium Cans for Wastewater Treatment**

A.L. Adejumo et al

- **Concomitant Administration of Quercetin and α -tocopherol Protects Rats from Cadmium Chloride Induced Neural Apoptosis and Cognitive Dysfunction**

Ali A. Shati

- **Structural Investigation of Semi Crystalline LDPE Nano-polymer**

M. S. Gaafar, H. Afifi and Kh. Al Zenidy

- **The Photogravitational Circular Restricted Four-body Problem with Variable Masses**

Abdullah A. Ansari